Aus der Klinik für Anaesthesiologie

der Ludwig-Maximilians-Universität München

Vorstand: Prof. Dr. med. Bernhard Zwißler

Dissertation
zum Erwerb des Doctor of Philosophy (Ph.D.)
an der Medizinischen Fakultät der
Ludwig-Maximilians-Universität zu München

A Micro-RNA-125a-Driven Functional Network Promotes Endothelial Permeability in Acute Inflammatory Conditions

vorgelegt von:

Lei Li

aus:

Hohhot, China

Jahr:

2022

Mit Genehmigung der Medizinischen Fakultät der
Ludwig-Maximilians-Universität zu München

First evaluator: Prof. Dr. Dr. Simone Kreth

Second evaluator: Priv. Doz. Dr. Patrick Möhnle

Third evaluator: Prof. Dr. Andreas Schober

Fourth evaluator: Priv. Doz. Dr. Tobias Petzold

Dean: **Prof. Dr. med. Thomas Gudermann**

Date of the defense:

20.07.2022

Content

List of figures

List of tables

List of abbreviations

3’UTR	Three Prime Untranslated Region
ADAMTS13	A Disintegrin and Metalloproteinase with A Thrombospondin Type 1 Motif, Member 13
ARDS	Acute Respiratory Distress Syndrome
BSA	Bovine Serum Albumin
cAMP	Cyclic Adenosine Monophosphate
cDNA	Complementary DNA
DGCR8	Digeorge Syndrome Critical Region 8
DIC	Disseminated Intravascular Coagulation
DMSO	Dimethyl Sulfoxide
dsRNA	Double-Stranded RNA
ECGM	Endothelial Cell Basal Medium
ECIS	Electric Cell-Substrate Impedance Sensing
ESAM	Endothelial Cell-Selective Adhesion Molecule
FCS	Fetal Calf Serum
FoxO1	Forkhead Box Protein O1
ICAMs	Intercellular Adhesion Molecules
IL-1	Interleukin-1
IL-6	Interleukin-6
JAMs	Junctional Adhesion Molecules

LPS	Lipopolysaccharide
MLCK	Myosin Light Chain Kinase
NF-κB	Nuclear Factor Kappa-Light-Chain-Enhancer of Activated B Cells
NGS	Next Generation Sequencing
PAI-1	Plasminogen Activator Inhibitor-1
PBS	Phosphate Buffered Saline
PCR	Polymerase Chain Reaction
PECAM-1	Platelet Endothelial Cell Adhesion Molecule-1
PP1	Protein Phosphatase 1
PPP1CA	Protein Phosphatase 1 Catalytic Subunit Alpha
PTP1B	Protein Tyrosine Phosphatase 1B
PTPN1	Protein Tyrosine Phosphatase Non-Receptor Type 1
RAC	Rac Family Small Gtpase
RISC	RNA-Induced Silencing Complex
SDS	Sodium Dodecyl Sulfate
TLR	Toll Like Receptor
TNF	Tumor Necrosis Factor
VCAM-1	Vascular Cell Adhesion Molecule-1
VE-cadherin	Vascular Endothelial-Cadherin
VEGF	Vascular Endothelial Growth Factor
VWF	Von Willebrand Factor

ZO-1	Zonula Occludens-1

1 Introduction

1.1 Endothelium in acute inflammation

The vascular endothelium is composed of a single layer of endothelial cells that line the interior surface of blood vessels. Endothelial cells detect changes in hemodynamic forces and signals from circulating blood, facilitate the bidirectional flow of substances and fluid between the blood and surrounding tissues, and control the adhesion and migration of immune cells as gatekeepers[1]. The integrity of the endothelial function is essential for facilitating immune response and coagulation, regulating vascular tone, and maintaining a semi-permeable barrier[2, 3].

Acute inflammation is the response of the body to harmful stimuli, such as pathogen infection, and is characterized by recruitment of immune cells and activation of cytokine networks. Adhesion molecules, including selectins, integrins, intercellular adhesion molecules (ICAMs), vascular cell adhesion molecule-1 (VCAM-1), and platelet endothelial cell adhesion molecule-1 (PECAM-1) increase on the endothelial cell surface in response to inflammatory stimuli, which promote leucocyte trans-endothelial migration into injured tissues[4, 5]. Endothelial cells are not only the target of cytokines produced by immune cells. Moreover, upon stimulation by bacterial endotoxin lipopolysaccharide (LPS) via TLR4/NF-κB signaling pathway, they can secrete cytokines, such as interleukin-1(IL-1), IL-6, and interferon[6, 7]. Thus, endothelial cells are active components of the networks modulating the immune response during acute inflammation.

Besides activating the inflammatory system, endothelial cells express adhesion molecules that trigger the clotting cascade during inflammation. Inflammatory stimuli such as IL-6 and VWF proteolytic fragment and thrombin inactivate ADAMTS-13,

which cleave von Willebrand factor multimers, and initiate thrombogenesis[8, 9]. During overwhelming inflammation, endothelial cells release plasminogen activator inhibitor-1 (PAI-1) to suppress the fibrinolytic pathway[10]. All together increase the risk of disseminated intravascular coagulation (DIC).

Barrier function is a natural attribute of endothelial cells, a selective endothelial barrier is crucial for maintaining fluid homeostasis[11, 12]. In acute inflammation, one of the main features of endothelial cells is the loss of barrier function and result in tissue edema[13].

1.2 Inflammation increases vascular permeability

Endothelial cells control the flow of molecules and fluid across the monolayer by highly regulated transport pathways to maintain tissue fluid and circulation homeostasis. The transport across the endothelium generally consists of transcellular and paracellular pathways[14], the latter plays a major role in the context of inflammation.

During systemic inflammation, vascular endothelial cells are among the first cell types in the body that expose and respond to a complex composition of inflammatory factors. One of the most common effects of these permeability-increasing agents or inflammatory cytokines is to induce intracellular signals that can cause the formation of inter-endothelial gaps[7, 15]. Cells or solutes flow across the endothelial barrier in an unrestricted manner which can lead to extracellular edema.

Increased endothelial permeability is a prominent feature of inflammatory diseases, where leakage can result in edema, impaired tissue function, and morbidity. Sepsis and acute respiratory distress syndrome (ARDS) are two examples of acute inflammatory diseases. In particular, septic shock characterized by systemic circulatory failure is accompanied by a complex endothelial dysfunction including the disruption of the

endothelial barrier, which further promotes edema and organ damage[16]. ARDS is a severe hypoxemic failure of the lungs, characterized by damage of the capillary endothelium and alveolar epithelium, which leads to the impaired gas exchange between the alveoli and the capillaries[17]. Sepsis, ARDS, and the frequently associated failure of organs show high mortality and become the leading causes of death in intensive care units around the world[17, 18]. Current management of these acute inflammatory diseases relies on infection source control, antimicrobial therapy, and restoration of tissue perfusion via fluid resuscitation[19, 20]. For endothelial barrier dysfunction, however, no specific treatment is currently available. The essential role of the endothelial barrier in the pathophysiology of acute inflammatory diseases highlights the need for a better understanding of the molecular mechanisms that maintain homeostasis of the endothelium.

1.3 Endothelial junctions

Endothelial cell junctions between neighboring cells are critical for vessel formation and maintenance, regulating tissue perfusion and endothelial barrier function in a dynamic manner. Endothelial junctions contain adherens junctions, tight junctions，and gap junctions, which connect adjacent cells and mediate cell-to-cell communication[12, 21]. Both adherens junctions and tight junctions are mediated by transmembrane proteins. Adherens junctions control permeability for large molecular weight components[22], in contrast, tight junctions are generally considered to control ions and small molecules permeability[23].

Other proteins found at endothelial junctions such as the platelet endothelial cell adhesion molecules (PECAMs) and the junctional adhesion molecules (JAMs) were proposed to contribute to regulating paracellular permeability in an indirect way by facilitating leukocyte recruitment and transmigration[24].

1.3.1 Adherens junctions

Vascular endothelial (VE)-cadherin is the central component of endothelial adherens junctions, joins neighboring endothelial cells through homophilic interactions, maintains the integrity of the endothelial barrier, and controls leukocyte extravasation [25, 26]. The cytoplasmic domain of VE-cadherin recruits catenins (mainly β- catenins and p120-catenins), which bind to α-actinin, thereby building the connection between adherens junctions and the actin cytoskeleton[27]. In confluent endothelial cells, the tyrosine phosphorylation of VE-cadherin and β-catenin are strongly reduced[28], the expression of VE-cadherin at the junctions of confluent endothelial cells inhibits the nuclear translocation and signal transduction of β-catenin [29]. The link of adherens junctions to actin promotes endothelial junction maturation and dynamic remodeling[30]. Additionally, VE-cadherin plays a role in transmitting intracellular signals, promotes cell survival, and regulating contact inhibition of cell growth[31, 32].

1.3.2 Tight junctions

Tight junctions are unevenly distributed throughout the vasculature and play the most prominent role at the blood-brain barrier and the blood-retina barrier. Endothelial cell tight junctions are composed of claudins, junction-associated molecule (JAM) families, endothelial cell-selective adhesion molecule (ESAM), and other adhesion molecules[33]. These junction proteins regulate the paracellular permeability of endothelium between adjacent cells[34].

Claudins are integral membrane proteins and are the central components of endothelial tight junctions[35]. Claudins consist of four membrane-spanning regions, including two extracellular loops and one intracellular loop[36]. Claudin-5 is not required for vascular

development in the embryo, brain microvasculature morphologic of claudin-5-null mice are normal but cannot establish a functional blood-brain barrier[37-39].

JAMs are not only expressed on the endothelium, but also on leukocytes. Here, their roles in modulating leukocyte adhesion and extravasation are well studied[40]. In endothelial cells, JAM-A increases claudin-5 expression and enhances endothelial barrier function[41]. ESAM assists VE-cadherin functions in lung microvasculature and controls plasma leakage[42].

1.4 Signaling of endothelial activation

Inflammation-induced endothelial activation and hyperpermeability is initiated by a great variety of stimuli generated and released from monocytes, platelets, mast cells, and endothelial cells[43]. The dynamic reactions of endothelial junctions are required to mediate adaptive responses. Hyperpermeability is characterized by the disruption of endothelial junctions and the activation of the contractile cell machinery, which leads to the loss of adhesive forces between adjacent cells[44]. The effects of pro-inflammatory stimuli on endothelium could be transient and reversible, such as histamine and thrombin. Other inflammatory cytokines, like tumor necrosis factor (TNF) and vascular endothelial growth factor (VEGF), induce long-lasting responses[45]. Of interest, most of these stimuli are produced in situations of acute inflammation.

In general, two key mechanisms are involved in regulating endothelial barrier disruption under inflammatory conditions. (I) Destabilization of endothelial adhesion junctions, which in most cases initiated by tyrosine phosphorylation induced disassembly and internalization of VE-cadherin[25]. (II) The activation of actin-myosin complex contractile machinery by myosin phosphorylation and cytoskeletal protein

remodeling, which is characterized by reorganization of cortical actin into cytosolic stress fibers[46]. All these factors together cause the disruption of endothelial junctions and the formation of inter-endothelial gaps, which impair the endothelial barrier function and induce vascular leakage.

A growing number of molecules was detected to modulate VE-cadherin expression, stability on the cell surface, phosphorylation, internalization, and signaling in response to inflammation.

Upon inflammatory stimulation, the levels of transcription factors that are crucial for VE-cadherin transcription and the formation of the adherens junctions are changed. For example, the cAMP response element binding (CREB) expression decreased in LPS-induced sepsis and consequently reduced CREB-mediated transcription of VE-cadherin[47]. Upon TNF activation, endothelial cells compensate for surface VE-cadherin degradation by upregulating its transcription factor ETS1 in an NF-κB dependent manner and promoting VE-cadherin de novo synthesis[48]. Thus, these transcription factors affect paracellular permeability by regulating VE-cadherin expression in response to inflammatory stimulation.

Inflammatory mediators activate tyrosine phosphorylation of VE-cadherin and catenins, play a role in moment-by-moment remodeling of adherens junctions[49]. In these cases, endothelial cells remain confluent and most of the junctional architecture is preserved, but the permeability of the monolayer is significantly increased[50]. Inflammatory stimuli suppress cAMP/RAC1 signaling, activate Rho and kinases such as Scr and Pyk2, leading to phosphorylation of VE-cadherin, which is then disassembled from p120-catenin, and internalized[51-53].

Hyperpermeability inducing factors such as TNF, histamine, and thrombin activate specific receptors in endothelial cells and increase the intracellular Ca^{2+} concentration.

This leads to activation of myosin light chain kinase (MLCK), which phosphorylates myosin regulatory light chain[54]. The phosphorylation of the myosin regulatory light chain promotes the interaction between myosin and cytoskeleton actin filaments, resulting in morphological remodeling and subsequent instability of adherens junction[55]. In contrast, the myosin light chain phosphatase removes the phosphate group from myosin and limits the disruption of the VE-cadherin junction complex[56].

Being an essential part of tight junctions, the role of claudin-5 in the blood-brain barrier has been deeply studied[57-59]. At the same time, its role in regulating the permeability of microvasculature during inflammation cannot be underestimated. Recent studies show that TNF could cause disruption of claudin-5 at endothelial tight junctions through activation of the NF-κB pathway[60]. Recent studies provide a growing body of evidence suggesting that adherens junctions and tight junctions are positively interconnected, the crosstalk between these two types of junctions regulates vascular barrier function upon inflammatory stimulation[61]. In confluent endothelial cells, the clustering of VE-cadherin on the cell membrane induces the expression of claudin-5[29].

1.5 microRNAs

MicroRNAs (miRNAs) are a class of small, non-coding RNA molecules with a length of about 22 nucleotides. They post-transcriptionally regulate gene expression by directly binding to the 3’ untranslated regions of messenger RNA (mRNA) transcripts of their target genes via complementary base pairing, known as canonical interaction, or perform miRNA-mRNA regulation via non-canonical binding sites[62]. The miRNA-mRNA interaction leads either to translational repression or degradation of the target mRNA, thereby preventing the synthesis of active protein.

Most miRNAs are evolutionarily conserved and are abundant in different cell types, which suggests that they have important biological functions. In recent years, the role of miRNAs in the regulation of related biological processes is being studied in depth. It is assumed that miRNAs regulate up to thirty percent of all protein-coding genes in humans[63]. The epigenetic regulatory effects of miRNAs are not completely explainable by the interactions with a single target gene. In fact, a given miRNA could have multiple mRNA targets, and a given target could be regulated by different miRNAs[64]. In addition, miRNAs usually control multiple targets in one signaling pathway, thereby expanding their regulatory capacity and forming regulatory networks [65, 66]. The indirect effects of miRNAs via suppression of enzymes or transcription factors may occur. Therefore, the miRNA networks eventually result in a significant impact on cell functions, so that miRNAs not only play a vital role in homeostasis but also in pathological processes[67]. Thus, the inflammatory inducible expression of miRNAs could play an important role in regulating endothelial barrier function during inflammation[68].

1.5.1 Biogenesis of microRNA

MiRNA-coding genes locate either in introns of host genes, which they share regulatory elements and the primary transcripts, or lie in non-protein-coding regions, in this case, they have their own promoter or exist as a cluster containing several functionally cooperating miRNAs and are transcribed together, thus exerting synergistic action[69].

The transcription of miRNAs genes is carried out by RNA polymerase type II in the nucleus. RNA polymerase II binds to the promoter in the DNA sequence, and then is capped with 7-methylguanosine at 5’ end. After polyadenylation with poly-A tail, and splicing, the resulting transcript then becomes a hairpin-loop primary microRNA[70]. The primary transcript is processed by a microprocessor complex consisting of

DiGeorge Syndrome Critical Region 8 (DGCR8) that recognizes the double-stranded RNA (dsRNA) structure of the hairpin, and the enzyme Drosha, which is a protein that cuts RNA and creates precursor-miRNA (pre-miRNA) composed of about 70 nucleotides[71]. These pre-miRNAs are then exported from the nucleus into the cytoplasm with the help of exportin-5, which recognizes the overhang left by Drosha at the 3' end of the pre-miRNA[72].

In the cytoplasm, the pre-miRNA is cleaved by Dicer, an RNase III enzyme cuts off the loop connecting 5' and 3' ends of the hairpin, resulting in a miRNA duplex with a length of about 22 nucleotides. Usually, only one strand acts as a functional miRNA and interacts with its target mRNA in the RNA-induced silencing complex (RISC)[73].

1.5.2 MicroRNAs and endothelial barrier function

It has been indicated that miRNAs play an important role in controlling the response of the endothelium to inflammatory stimulation, including endothelial barrier function[74, 75]. Besides modulating the expression and functions of adhesion molecules by targeting the NF-κB pathway, the role of miRNAs in regulating endothelial barrier function via junction proteins has recently been proposed[76, 77].

VE-cadherin is the major component of endothelial adherens junctions. By directly targeting VE-cadherin, miR-27a plays a vital role in endothelial inflammation, angiogenesis, and vascular permeability. Furthermore, specific blocking of miR27a-dependent VE-cadherin repression promotes VE-cadherin localization at cell-cell junctions and inhibits endothelial permeability in vitro and VEGF-induced vascular leakage in mice[78]. Likewise, miR-22 and miR101 transcriptionally inhibit VE-cadherin expression and impact angiogenesis and permeability in vivo[79, 80].

A possible role of miRNAs in regulating endothelial barrier functions via targeting tight junctions during inflammation has also been revealed. Overexpression of miR-150-5p increased blood-tumor barrier permeability of glioma endothelial cells and decreased the expression of ZO-1, Occludin, and Claudin-5[81]. The absence of miR-150 in the endothelial cell or knockout of miR-150 in the mouse model caused an irreversible increase in vascular permeability. On the contrary, the upregulation of miR-150 expression in wild-type mice vasculature reduced Ang2 levels and decreased mortality due to sepsis[82].

These studies support the importance of miRNAs in regulating endothelial barrier function during inflammation and provide insights for the development of novel therapeutic targets for the management of endothelial barrier function. However, based on the functional characteristics of miRNAs, the regulatory effects of miRNAs cannot be completely explained by a single miRNA-target gene interaction. Much more, miRNAs target multiple genes, forming regulatory networks and potentiating their impact on cellular functions. Therefore, more efforts are needed to determine the miRNAs regulatory network that controls the permeability of endothelial cells[83].

1.5.3 The miR-125 family in inflammation

Among the most important miRNA families, the miR-125 family is highly conserved throughout diverse species and has been reported to play a pivotal role in a variety of cellular processes and diseases. miR-125 family consists of hsa-miR-125a, hsa-miR-125b-1 and hsa-miR-125b-2[84].

It has been found that microRNA-125a/b-5p inhibits the expression of vasoconstrictive peptides endothelin-1 in endothelial cells[85]. After VEGF stimulation, the expression of miR-125b in endothelial cells increased transiently and the barrier function was

impaired. By inhibiting the translation of VE-cadherin, miR-125b has been identified as an important regulator of vascular endothelial cell tube formation[86].

Recent studies revealed that the level of circulating miR-125a in the blood samples of patients with sepsis was elevated and is related to disease severity[87]. Due to the relevance of the miR-125 family and endothelial functions, we hypothesized that miR-125a may also be involved in regulating inflammatory endothelial barrier disruption and targeting miR-125a could provide a novel therapeutic approach.

1.5.4 Extracellular vesicles

Although the majority of miRNAs localized intracellularly, some miRNAs, commonly known as circulating miRNAs or extracellular miRNAs, are packaged in extracellular vesicles and released into body fluids, including blood, urine, atherosclerotic plaques, tumors, and have the potential to be diagnostic biomarkers in a number of diseases[88, 89]. Intracellular miRNAs are selectively packaged into extracellular vesicles and transferred to recipient cells[90]. By recognizing the binding sites in the 3'UTR of target mRNA and repressing protein expression, miRNAs modulate gene expression in recipient cells.

Under inflammatory stimulation, endothelial cells are not only the victims but also are able to actively modulate the immune response. In addition to interacting with other cells and tissues by expressing adhesion molecules on the cell surface and producing inflammatory cytokines, endothelial cells could release microparticles containing proteins, mRNAs, and miRNAs that are capable of regulating inflammation[91]. Investigators reported an increase in extracellular vesicles in patients with septic shock[92]. As a transcellular delivery system for microRNAs, extracellular vesicles play an active and important role in regulating pathophysiological changes during inflammation[93].

Studies have shown that miRNAs are differently enriched in extracellular vesicles, and their expression patterns will vary with respect to different diseases. Therefore, extracellular miRNAs are considered as potential diagnostic biomarkers and therapeutic agents.

1.6 Aims of the study

Vascular endothelium forms a barrier between the circulation and surrounding tissues. Acute inflammatory processes such as sepsis are usually accompanied by a dysfunctional endothelial barrier, leading to the formation of edema, microcirculatory failure, and ultimately organ damage. A better understanding of the molecular mechanisms that maintain endothelial homeostasis in acute inflammation is necessary for the development of new therapeutic concepts.

In the past few years, miRNAs have gained attention as regulators of endothelial barrier function and were proved to play an essential role in regulating the expression of adhesion molecules, especially in the context of acute inflammatory insults. Recent studies have shown that circulating miR-125a is upregulated in the blood of patients with acute vascular diseases. Thus, we hypothesized that miR-125a may be involved in regulating inflammatory endothelial barrier disruption.

Therefore, this research aimed to study:

1. Whether the expression level of miR-125a in endothelial cells is inducible in the inflammatory microenvironment.

2. Whether inflammation-induced miR-125a affects the endothelial barrier destruction, and whether inhibition of miR-125a could rescue the hyperpermeable phenotype.

3. Whether miR-125a regulates endothelial barrier function by establishing a specific regulatory network and which target genes are included.

2 Materials and Methods

2.1 Materials

All materials used for the preparation of the dissertation and their manufacturers are listed in alphabetical order below.

2.1.1 Laboratory equipment

Apollo 200 Nitrogen Tank	Cryotherm, Kirchen (Sieg)
BDK Laminar Flow Safety Workbench	Luft- und Reinraumtechnik GmbH, Pfullinger
Buhler Shaker	Edmund Bühler GmbH, Hechingen
BVC 21 Suction Pump	Vacuubrand, Wertheim
Capnomac Ultima	GE Healthcare Europe GmbH, Freiburg
Centrifuge 5415R	Eppendorf AG, Hamburg
Centrifuge 5424R	Eppendorf AG, Hamburg
Digital Imager	Hamamatsu Photonics, Hamatsu, Japan
E-BOX VX2 Gel Documentation System	Peqlab Biotechnologie GmbH, Erlangen
Electric Cell-Substrate Impedance Sensing (ECIS)® Z	Applied BioPhysics, Troy, NY, USA
FilterMax F3 MultiMode Microplate Reader	Molecular Devices, Sunnyvale, USA
Fine Balance MP 300	Chyo Balance Corp., Kyoto, Japan
Heraeus Megafuge 40R Centrifuge	Thermo Scientific, Schwerte
Heraeus Rotina 35R	Thermo Scientific, Schwerte
Hettich Mikro 200 centrifuge	Andreas Hettich GmbH, Tuttlingen

Incubator	Binder GmbH, Tuttlingen
Incubator	Heraeus, Hanau
Incubator	Thermo Fisher, Waltham, MA, USA
LEICA-TCS SP5 Confocal Microscope	Leica, Wetzlar
Light Cycler® 480 II	Roche Diagnostics GmbH, Mannheim
Mastercycler® Gradient	Eppendorf AG, Hamburg
Medical Carbon Dioxide LAPAROX ®	Linde AG, Pullach
Milli-Q Advantage A10 Water System	Merck KGaA, Darmstadt
Mini-PROTEAN® System Casting Stand	Bio-Rad Laboratories Inc., Hercules, USA
Modular Incubator Chamber	Billups-Rothenberg Inc., Del Mar, USA
NALGENE™ Cryo 1 °C Freezing Container	Thermo Scientific, Schwerte
NanoDrop™ NC-2000	Peqlab Biotechnologie GmbH, Erlangen
Neon™ Transfection System	Invitrogen GmbH, Darmstadt
Nitrogen	Linde AG, Pullach
Olympus IX50 Inverted Phase Contrast Microscope	OLYMPUS EUROPA SE & CO. KG,Hamburg
Pipettes	Eppendorf AG, Hamburg
Polymax 1040	Heidolph Instruments GmbH & Co. KG, Schwabach
RCT Basic Magnetic Stirrer	IKA-Werke, Staufen
SevenEasy pH	Mettler-Toledo AG, Schwerzenbach, Switzerland
Shaker ST-3	neoLab Migge, Heidelberg
Standard Power Pack P25	Biometra GmbH, Göttingen
Sub-Cell GT Electrophoresis System	Bio-Rad Laboratories Inc., Hercules, USA

Thermo-Shaker	CUSABIO, Wuhan, China
Trans-Blot® Turbo™ Transfer System	Bio-Rad Laboratories Inc., Hercules, USA
Ultracentrifuge TGA-50	Hemotec, Gellerkirchen, Schweiz
Ultrasonic Homogenizer	Reitz Medical GmbH, Rosenheim
Vac-Man® Laboratory Vacuum Manifold	Promega GmbH, Mannheim
Vacuum Pump	ILMVAC GmbH, Ilmenau
vapo.protect	Eppendorf AG, Hamburg
Vi-Cell XR Cell Viability Analyzer	Beckman Coulter Inc., Fullerton, USA
VWR Digital Vortex Mixer	VWR International, Leuven, Belgium
Water Bath B3	Haake Technik GmbH, Vreden
Water Bath SWB 25	Haake Technik GmbH, Vreden

2.1.2 Chemicals, reagents, and antibodies

2-Mercaptoethanol	Sigma-Aldrich, St. Louis, USA
2 × Laemmli Sample Buffer	Bio-Rad Laboratories Inc., Hercules, USA
Acrylamide/Bis Solution (30%)	Sigma-Aldrich, St. Louis, USA
Agar	AppliChem GmbH, Darmstadt
Agarose SERVA Tablets 0.5 g/tablet	Serva Electrophoresis GmbH, Heidelberg
Albumin-Fluorescein Isothiocyanate Conjugate	Sigma-Aldrich, St. Louis, USA
alpha-actinin-4 Antibody (A-8)	Santa Cruz Biotechnology, USA
Ammonium Persulfate	Bio-Rad Laboratories Inc., Hercules, USA
Ampicillin-Sodium salt	AppliChem GmbH, Darmstadt
Anti-miR™ Negative Control #1	Thermo Fisher Scientific, Waltham, MA, USA

Anti-mouse IgG, HRP-linked Antibody #7076	Cell Signaling Technology, Danvers, USA
Anti-rabbit IgG, HRP-linked Antibody #7074	Cell Signaling Technology, Danvers, USA
Aqua	Berlin-Chemie AG, Berlin
Bovine Serum Albumin (BSA)	Carl Roth GmbH, Karlsruhe
Chloroform	Sigma-Aldrich Chemie GmbH, Steinheim
Clarity and Clarity Max Western ECL Substrates	Bio-Rad Laboratories Inc., Hercules, USA
Claudin-5 Antibody (A-12)	Santa Cruz Biotechnology, USA
CutSmart® Buffer	New England Biolabs Inc., Ipswich, USA
Deoxynucleoside Triphosphate Set (dNTPs)	Roche Diagnostics GmbH, Mannheim
Dimethyl Sulfoxide (DMSO) cell culture grade	Sigma-Aldrich Chemie GmbH, Steinheim
DNA Ladder 100 bp	Promega GmbH, Mannheim
DNA Ladder 1 kb	Thermo Scientific, Schwerte
Dulbecco's Modified Eagle Medium (DMEM)	Gibco, Grand Island, NY, USA
ECGM SupplementMix	PromoCell, Heidelberg
Endothelial Cell Basal Medium (ECGM)	PromoCell, Heidelberg
Ethanol absolute	VWR Chemicals, Leuven, Belgium
Ethidium Bromide	SERVA Electrophoresis GmbH, Heidelberg
Ets-1 Antibody (C-4)	Santa Cruz Biotechnology, USA
FastStart Essential DNA Probes Master	Roche Diagnostics GmbH, Mannheim
Fetal Calf Serum (FCS)	Biochrom AG, Berlin
Gel Loading Dye Purple (6×)	New England Biolabs Inc., Ipswich, USA

Gelatine	Merck KGaA, Darmstadt
Glutaraldehyde	Sigma-Aldrich Chemie GmbH, Steinheim
Glycine	Bio-Rad Laboratories Inc., Hercules, USA
Goat anti-Mouse IgG (H+L) Highly Cross-Adsorbed Secondary Antibody, Alexa Fluor 488	Thermo Fisher Scientific, Waltham, MA, USA
Hank's Balanced Salt Solution	Apotheke Klinikum der Universität München, Munich
hsa-miR-125 mirVana™ miRNA inhibitor	Thermo Fisher Scientific, Waltham, MA, USA
hsa-miR125 premiR miRNA	Thermo Fisher Scientific, Waltham, MA, USA
Human IFN-γ	Miltenyi Biotec, Bergisch Gladbach
Human TNF-α	Miltenyi Biotec, Bergisch Gladbach
Hydrochloric Acid (HCl)	Sigma-Aldrich Chemie GmbH, Steinheim
Ibidi Mounting Medium	Ibidi, Gräfelfing
Isopropanol	Sigma-Aldrich Chemie GmbH, Steinheim
L-Glutamine 200 mM	Biochrom AG, Berlin
MEM Non-essential Amino Acids (NEAA) (100×)	Life Technologies GmbH, Darmstadt
Methanol	Merck KGaA, Darmstadt
Nonfat dry milk Blotting Grade Blocker	Bio-Rad Laboratories Inc., Hercules, USA
NotI-HF®	New England Biolabs Inc., Ipswich, USA
Oligo- Deoxythymidine (Oligo-(dT)) Primer	Qiagen GmbH, Hilden
ON-TARGETplus Control Pool Non-	Dharmacon, Lafayette, CO, USA

Targeting Pool (siNC)	
ON-TARGETplus siRNA-SMARTpool Human CDH5	Dharmacon, Lafayette, CO, USA
ON-TARGETplus siRNA-SMARTpool Human CLDN5	Dharmacon, Lafayette, CO, USA
ON-TARGETplus siRNA-SMARTpool Human ETS1	Dharmacon, Lafayette, CO, USA
ON-TARGETplus siRNA-SMARTpool Human PPP1CA	Dharmacon, Lafayette, CO, USA
ON-TARGETplus siRNA-SMARTpool Human PTPN1	Dharmacon, Lafayette, CO, USA
PageRuler Plus Prestained Protein Ladder	Thermo Scientific, Schwerte
Paraformaldehyde	Sigma-Aldrich Chemie GmbH, Steinheim
Penicillin-Streptomycin (10,000 U/ml)	Gibco, Grand Island, NY, USA
peqGREEN DNA and RNA Dye	Peqlab Biotechnologie GmbH, Erlangen
Phosphatase Inhibitor Cocktail (100×)	Cell Signaling Technology, Danvers, USA
Phosphate Buffered Saline (PBS)	Apotheke Klinikum der Universität München
Phospho-VE-cadherin (Tyr658) Polyclonal Antibody	Thermo Fisher Scientific, Waltham, MA, USA
Pierce™ RIPA Buffer	Thermo Scientific, Schwerte
Poly-L-Lysine	Merck KGaA, Darmstadt
PP1α Antibody (G-4)	Santa Cruz Biotechnology, USA
Pre-miR™ Negative Control #1	Thermo Fisher Scientific, Waltham, MA, USA
Protease Inhibitor Cocktail (100×)	Cell Signaling Technology, Danvers, USA
psiCHECK™-2 Vector	Promega GmbH, Mannheim

PTP1B (D-4) Antibody (D-4)	Santa Cruz Biotechnology, USA
Purified BSA 100×	New England Biolabs Inc., Ipswich, USA
QIAzol® Lysis Reagent	Qiagen GmbH, Hilden
QuikChange® XL10-Gold Ultracompetent Cells	Stratagene, Inc., La Jolla, USA
Rac2 Antibody (AT2G11)	Santa Cruz Biotechnology, USA
Random Hexamers	Qiagen GmbH, Hilden
RNaseOUT™ Recombinant Ribonuclease Inhibitor	Life Technologies GmbH, Darmstadt
Rotiphorese® 10× TAE-Buffer	Carl Roth GmbH, Karlsruhe
Sodium Chloride (NaCl)	Merck KGaA, Darmstadt
Sodium Dodecyl Sulfate (SDS)	Roche Diagnostics GmbH, Mannheim
Sodium Pyruvate (100 mM)	PAA Laboratories GmbH, Pasching, Austria
Strata Clone™ Solo Pack® Competent Cells	Stratagene, Inc., La Jolla, USA
SuperScript™ III Reverse Transcriptase	Invitrogen, Waltham, MA, USA
T4 DNA Ligase	Roche Diagnostics GmbH, Mannheim
T4 DNA Ligase Buffer	Roche Diagnostics GmbH, Mannheim
TEMED	Bio-Rad Laboratories Inc., Hercules, USA
To-Pro®3 iodide (642/661)	Life Technologies GmbH, Darmstadt
TRIS	Bio-Rad Laboratories Inc., Hercules, USA
TRIS-HCl	Bio-Rad Laboratories Inc., Hercules, USA
Triton™ X-100	Sigma-Aldrich Chemie GmbH, Steinheim

Trypsin/Ethylenediaminetetraacetate (EDTA) Solution	Biochrom AG, Berlin
Tryptone	AppliChem GmbH, Darmstadt
Tween 20	Sigma-Aldrich Chemie GmbH, Steinheim
VE-Cadherin Antibody (F-8)	Santa Cruz Biotechnology, USA
XhoI	New England Biolabs Inc., Ipswich, USA
Yeast Extract Molecular Biology Grade	AppliChem GmbH, Darmstadt
β-Actin (13E5) Rabbit mAb	Cell Signaling Technology, Danvers, USA

2.1.3 Commercial kits

Dual-Glo Luciferase Assay System	Promega GmbH, Mannheim
esoRNeasy Midi Kit	Qiagen GmbH, Hilden
miRNeasy Mini Kit	Qiagen GmbH, Hilden
miRNeasy Serum/Plasma Kit	Qiagen GmbH, Hilden
Monarch DNA Gel Extraction Kit	New England Biolabs Inc., Ipswich, USA
Neon™ Transfection System 100 µl Kit	Invitrogen GmbH, Darmstadt
Neon™ Transfection System 10 µl Kit	Invitrogen GmbH, Darmstadt
peqGOLD Plasmid Miniprep Kit I	Qiagen GmbH, Hilden
Pierce Bicinchoninic acid (BCA) Protein Assay Kit	Thermo Scientific, Schwerte
Pure Yield Plasmid Midiprep System	Promega GmbH, Mannheim
QuikChange Lightning Multi Site-Directed Mutagenesis Kit	Agilent Technologies, Santa Clara, USA
Rapid DNA Dephos & Ligation Kit	Roche Diagnostics GmbH, Mannheim

RNase-free DNase Set	Qiagen GmbH, Hilden
Spectra Multicolor Broad Range Protein Ladder	Thermo Scientific, Schwerte
StrataClone Ultra Blunt *Polymerase Chain Reaction* (PCR) Cloning Kit	Agilent Technologies, Santa Clara, USA
SuperScript III Reverse Transcriptase Kit	Life Technologies GmbH, Darmstadt
TaqMan® MicroRNA Assay, Assay Name: U47, hsa-miR-125a-5p	Life Technologies GmbH, Darmstadt
TaqMan® MicroRNA Reverse Transcription Kit	Life Technologies GmbH, Darmstadt
Trans-Blot® Turbo™ Transfer Pack	Bio-Rad Laboratories Inc., Hercules, USA
Turbo DNA-Free Kit	Life Technologies GmbH, Darmstadt

2.1.4 Disposable materials

0.2 ml Multiply®-Pro cup	Sarstedt, Nümbrecht
1.5 ml Micro Tube	Sarstedt, Nümbrecht
1.6 ml DNase, RNase free Tube	Biozym Scientific GmbH , Hessisch Oldendorf
1.6 ml DNase, RNase free Tube, Blue	Biozym Scientific GmbH , Hessisch Oldendorf
2.0 ml DNase, RNase free Tube	Sarstedt, Nümbrecht
Autoclaved Pipette Tip (0.5-10 µl, 0.5-20 µl, 2-200 µl, 100-1000 µl)	Eppendorf, Hamburg
Cell Culture Dish, 100 × 20 mm	Eppendorf, Hamburg
Cell Culture Flask 25 cm², 75 cm², 175 cm²	Greiner Bio-One, Frickhausen
Cell Culture Inserts (pore size 0.4 µm)	Greiner Bio-One, Frickhausen
Cell Culture Microplate, 96-well, PS, F-Bottom, White	Greiner Bio-One, Frickhausen

Cell Culture Plate, 6-well, 12-well, 24-well	Greiner Bio-One, Frickhausen
CryoTube™ Vials	Thermo Scientific, Schwerte
Delta Disposable Cell Spreader sterile	Heathrow Scientific LLC, Vernon Hills, USA
ECIS Cultureware 8W10E+ PET	Ibidi, Gräfelfing
Falcon 50 ml	Greiner Bio-One, Frickhausen
Filter Tips (0.5-20 µl, 2- 200 µl, 100-1000 µl, 1000-5000 µl)	Eppendorf, Hamburg
Glass pasteur pipette 150 mm	A.Hartenstein Laborbedarf GmbH, Würzburg
Inoculation loop 1 µl white	Sarstedt, Nümbrecht
Laboratory Glass Bottles	DURAN Group GmbH, Wertheim
Light Cycler 480 multiwell Plate 96, white	Roche Diagnostics GmbH, Mannheim
Mini-Protean 3 System Glass Plates	Bio-Rad Laboratories Inc., Hercules, USA
Multidirectional Stopcock for infusion	Braun Melsungen AG, Melsungen
Nunc 96-well Cell Culture Plate, black	Thermo Fisher Scientific, Massachusetts, USA
Safe Lock Tube 0.5 ml	Eppendorf, Hamburg
Serological pipettes (5 ml, 10 ml, 25 ml, 50 ml)	Eppendorf, Hamburg
Trans-Blot® Turbo™ TransferPack	Bio-Rad Laboratories Inc., Hercules, USA
Tube, 13 ml	Sarstedt, Nümbrecht
Vi-Cell Counting Cup	Beckman Coulter, Krefeld
µ-Slides I 0.4 Luer	Ibidi, Gräfelfing

2.1.5 Medium, gels, and buffer

Medium

ECGM- Culture Medium

Endothelial Cell Basal Medium	500 ml
FCS (heat inactivated)	10%
Endothelial Cell Growth Supplement	0.004 ml/ml
Epidermal Growth Factor (recombinant human)	0.1 ng/ml
Basic Fibroblast Growth Factor (recombinant human)	1 ng/ml
Heparin	90 µg/ml
Hydrocortisone	1 µg/ml
Penicillin-Streptomycin	1%

DMEM-Medium (HEK-Medium; Dulbeccos' Modified Eagle Medium)

DMEM-Medium	500 ml
FCS (heat inactivated)	10%
L-Glutamine	1%
Penicillin-Streptomycin	1%
NEAA	1%

LB-Medium (Luria Bertani Medium)

Tryptone	5 g
Sodium Chloride	5 g
Yeast Extract Molecular Biology Grade	2.5 g
ddH_2O	500 ml

LB-Agar (Luria Bertani Agar)

Tryptone	5 g
Sodium Chloride	5 g

Yeast Extract Molecular Biology Grade	2.5 g
Agar	7.5 g
ddH_2O	500 ml

Gels

1% Agarose Gel

Agarose	1 g
TAE-Buffer	100 ml
peqGREEN DNA and RNA Dye	5 µl

SDS Polyacrylamide Gels

	Separating Gel (12%)	Stacking Gel (4%)
ddH20	3.04 ml	1.89 ml
Separating Gel Buffer (1.5 M Tris, pH 8.8)	1.75 ml	-
Stacking Gel Buffer (0.5 M Tris, pH 6.8)	-	325 µl
10% SDS	91 µl	26 µl
30% Acrylamide/Bis Solution	3.64 ml	346 µl
40% APS	35 µl	10 µl
Temed	2.9 µl	2 µl

Buffer

Complete Lysis Buffer	1% Phosphatase Inhibitor Cocktail, and 1% Protease Inhibitor Cocktail in RIPA Buffer

Blocking Buffer	5% Nonfat dry milk Blotting Grade Blocker in TBS-T	
10 × SDS running buffer	Tris	250 mM
	Glycine	1.92 M
	SDS	1%
TBS-T (pH 7.5, adjust with HCl)	Tris	20 mM
	Sodium Chloride	150 MM
	Tween 20	0.1%
Stripping Buffer (pH 2.2, adjust with HCl)	Glycine	1.5 g
	SDS	0.1 g
	Tween 20	1 ml
	ddH_2O	100 ml
2 × Laemmli Sample Buffer	2-Mercaptoethanol	50 µl
	2× Laemmli Sample Buffer	950 µl

2.1.6 Oligonucleotides

All oligonucleotides used were synthesized by Metabion, Martinsried. The Universal ProbeLibrary (UPL) probes and single assays were obtained from Roche Diagnostics GmbH, Mannheim.

Table 1 Primer sequences and UPL probe numbers for qPCR

Target Name	UPL Probe Number	Primer Sequence
ACTN4	42	forward: 5’-AAATACCTCGACATCCCCAAG-3’ reverse:5’-GGTCATTATGGCCTTCTCG-3’
CDH5	58	forward: 5’-AAGCCTCTGATTGGCACAGT-3’ reverse:5’-CTGGCCCTTGTCACTGGT-3’
CLDN5	19	forward: 5’-CCATGGGATGAGAGAGACAGT-3’ reverse:5’-GGCCCTTTCTCGCACTCT-3’
ETS1	3	forward: 5’-GCAGAATGAGCTACTTTGTGGA-3’ reverse:5’-TTGCTAGGTCCTTGCCTCAC-3’
GAPDH	60	forward: 5’-AGCCACATCGCTCAGACAC-3’ reverse:5’-GCCCAATACGACCAAATCC-3’
PPP1CA	40	forward: 5’-GACAGCGAGAAGCTCAACCT-3’ reverse:5’-CGCGGATCTCGTTCTCTG-3’
PTPN1	32	forward: 5’-CGGTCACTTTTGGGAGATG-3’ reverse:5’-GCCAGTATTGTGCGCATTT-3’
RAC2	77	forward: 5’-GATGCAGGCCATCAAGTGT-3’ reverse:5’-CTGATGAGAAGGCAGGTCTTG-3’

TBP	87	forward: 5’-GAACATCATGGATCAGAACAACA-3’ reverse:5’-ATAGGGATTCCGGGAGTCAT-3’

Table 2 Primer sequences for Cloning

Gene		Sequence	Restriction Site
ACTN4	forward	5’-AGAGACTAGCCCCAGACAG-3’	Xho1: CTCGAG
	reverse	5’-CCACTGGCAAGGAGAAAGC-3’	Not1: GCGGCCGC
PTPN1	forward	5’-TGGTGGGAACATTCGAGGTG-3’	Xho1: CTCGAG
	reverse	5’-GGCAAAGCGTCAATTTGGGA-3’	Not1: GCGGCCGC
RAC2	forward	5’-AGATGGGTCTGATCCTCCAG-3’	Xho1: CTCGAG
	reverse	5’-AAAAGTCCTGACTGGCAAGG-3’	Not1: GCGGCCGC

Table 3 Primer sequences for Mutagenesis

Gene		Sequence
PTPN1	forward	5’-GGGGGGGAGTGTCTCACAGTCTTCTGTGACC-3’
	reverse	5’-GGTCACAGAAGACTGTGAGACACTCCCCCCC-3’

2.2 Methods

2.2.1 Cell culture

2.2.1.1 Isolation of human umbilical vein endothelial cells (HUVEC)

Human Umbilical Vein Endothelial Cells (HUVEC) were isolated from umbilical cords of healthy neonates directly after cesarean section at the Department of Gynecology and Obstetrics, University Hospital, LMU Munich. After the donors had given their written informed consent, the umbilical cord was placed in a container filled with 50 mL sterile PBS with 1% penicillin/streptomycin and processed immediately.

The umbilical cord was placed in a glass dish and squeezed out the blood, fresh cuts were made on both ends of the cord. Blunt cannulas were inserted into the vein and tightened with plastic straps. Cannulas were clamped with a hemostat and a 20 mL syringe of Hank's Balanced Salt Solution (HBSS) was attached to the cannula by a stopcock. The vein was washed with HBSS and filled with a few milliliters of HBSS to check for leaks. Then the umbilical cord was transferred to a new dish, injected approximately 10 mL 1% collagenase solution in HBSS to fill the umbilical vein until there was moderate distention of the vein. The stopcocks were closed, and the cord was incubated at 37 °C for 10 minutes. After incubation, the cord was taken out and fluid in the umbilical vein was collected into a 50 mL Falcon. The vein was then rinsed with M199 medium to collect the remaining detached endothelial cells. The cell suspension was spun at 1200 rpm for 5 minutes and the pellet was resuspended in ECGM culture medium, then seeded in a cell culture dish. Cells were incubated at 37 °C with 5% CO_2 overnight. The culture medium was changed the next day and continued incubation until the cell culture dish was confluent (1-4 days).

2.2.1.2 Cell splitting

HUVEC of one single cord at passage 2-4 were used for each of the experiments. Depending on the growth, the cells were subcultured every two to three days. When HUVEC monolayers reached 80% confluence, the medium was discarded, dead cells were rinsed off with PBS. HUVEC were detached from the culture dish with 1 × trypsin/EDTA during a one-minute incubation in the incubator. Trypsin/EDTA was inactivated with 3 mL ECGM medium, the cell suspension was collected into a 50 mL Falcon and spun at 1200 rpm for 5 minutes. The supernatant was removed, and the cell pellet was resuspended in 1mL PBS. The cell count and viability were measured by the Vi-Cell™ XR Cell Viability Analyzer using trypan blue staining. Only cells with a viability of > 85% were used for the experiments. Depending on the number of cells to be recultivated, the corresponding cell suspension volume was distributed into new cell culture dishes and cultivated at 37 °C, 5% CO_2.

2.2.1.3 Cryopreservation

For cryopreservation, HUVEC were preserved at their first passage. HUVEC were detached from the cell culture dish as described above. After counting, 1×10^6 cells in 1 mL cryopreservation solution were distributed in each CryoTube™ vial. The cryopreservation solution consists of 90% FCS and 10% DMSO. Immediately afterward, these vials were transferred in a freezing container filled with 2-propanol and stored in a -80 °C refrigerator to achieve a steady rate of cooling (-1 °C per hour). Then the cells were transferred to the liquid nitrogen tank for long-term preservation.

When thawing cells, the cryovial containing the frozen cells was removed from liquid nitrogen storage and immediately placed into a 37°C water bath. The vial was transferred into a laminar flow hood when there was just a small bit of ice left. 500 µL pre-warmed ECGM culture medium was added into each vial and the cell suspension

was distributed equally into two culture dishes containing 5 ml ECGM culture medium. Cells were incubated at 37 °C with 5% CO_2 for 2 hours. When cells attached to the culture dish, the medium was changed afterward to remove DMSO and continued incubation until the cells were ready to be subcultured.

2.2.1.4 Cell culture of HEK-293 cells

HEK-293 cells were purchased from the American Type Cell Culture Collection and cultured in DMEM medium. Cells were cultured at 37°C and 5% CO_2. HEK-293 cells used for experiments were not cultured beyond passage 20.

The HEK-293 cells stored in cryotubes were thawed quickly in a 37°C water bath, transferred to a sterile 50 mL Falcon with 10 ml DMEM medium and centrifuged at 1500 rpm for 3 minutes to wash out DMSO. After the supernatant had been removed, the cells were counted using Vi-Cell™ XR Cell Viability Analyzer. About 2×10^6 cells were then cultured in a 75 cm^2 cell culture flask with 10 mL DMEM medium containing 20% FCS overnight at 37 °C and 5% CO_2. On the following day, the medium was replaced with a 10% FCS-containing DMEM medium.

2.2.2 Induction of inflammatory conditions

In the inflammation-inducing experiments, 75,000 cells/well HUVEC were seeded in 24-well plates and incubated for 24 hours. When HUVEC monolayers reached approximately 80% confluence, cells were serum-starved with ECGM containing 0.5% FCS for 12 hours. For cytokine stimulation experiments with tumor necrosis factor (TNF) and interferon-gamma (IFN-γ), cells were then incubated in ECGM culture medium with 25 ng/mL TNF and 50 ng/mL IFN-γ for 4 hours. For hypoxia experiments, cells were incubated in ECGM culture medium supplemented with 25ng/mL TNF and incubated at 37 °C, 5% O_2, and 40 mmHg CO_2 in a humidified modular incubator

chamber for 24 hours.

2.2.3 Transfection of HUVEC

Transfections were conducted using the Neon™ electroporation system. Voltage pulses led to the temporary permeabilization of the cell membrane, which allowed a time-limited uptake of nucleic acids. The cells were harvested, centrifuged, and counted as described above. For subsequent investigations, a certain number of cells (see Table 1) were resuspended in Neon™ resuspension buffer R and transfected with hsa-miR125 pre-miR miRNA (pre-miR-125a), hsa-miR-125 miRNA inhibitor (miR-125a inhibitor), or respective siRNAs. Transfection of HUVEC was carried out at final concentrations of 50 nM (pre-miR-125a) or 100 nM (miR-125 inhibitor, siRNAs). As a control, Pre-miR™ Negative Control (NC pre-miR), Anti-miR™ Negative Control (NC anti-miR), or ON-TARGETplus Control Pool Non-targeting Pool (siNC) was transfected under the same conditions. The electroporation was carried out once for 30 ms at 1350 volt. The transfected HUVEC were then transferred to pre-warmed ECGM culture medium without antibiotics and cultured in the incubator at 37 °C and 5% CO_2.

Table 4 Experimental conditions of HUVEC transfection

Methods	Cell no.	Medium volume	Cell culture	Neon™ tip
qRT-PCR	3×10^5	2 mL	6-well	100 µL
Western Blot	2×10^5	1 mL	12-well	10 µL
FITC-BSA Passage	3×10^5	200 µL in insert 800 µL in well	24-well	100 µL

ECIS	1×10^5	400 µL	ECIS 8W10E+	10 µL
Immunofluorescence	1.5×10^5	100 µL	µ-Slides $I^{0.4}$ Luer	10 µL

2.2.4 Molecular biological methods

2.2.4.1 Purification of exosomes from cell culture supernatant

Purification and isolation of exosomal and other extracellular vesicles RNA from cell culture supernatants was conducted with exoRNeasy Serum/Plasma Midi Kit (Qiagen) according to the manufacturer's protocol. After collection, cell culture supernatant was spun at 3000 g for 15 minutes to exclude particles larger than 0.8 µm. The supernatant was then mixed with buffer XBP and bound to the column. Particulate matter such as larger protein complexes was removed during the binding step and the subsequent washing step. Lysis of vesicular RNA was facilitated by phenol/guanidine based QIAzol Lysis Reagent, which followed by silica-membrane purification of total RNA.

2.2.4.2 RNA isolation

Total RNA was isolated from HUVEC using the miRNeasy Mini kit according to the manufacturer's protocol. Cells were homogenized in 700 µL QIAzol Lysis Reagent and the mixture was vortexed for 15 seconds and placed at room temperature for 5 minutes. After the addition of 140 µL chloroform, the homogenate was separated into aqueous and organic phases by centrifugation for 15 minutes at 12,000 × g at 4 °C. RNA in the upper aqueous phase was collected and mixed with 1.5 volumes of 100% ethanol. The sample was then applied to the RNeasy Mini spin column. After washing with buffer

RWT for once, the spin column was incubated with 80µL DNase I incubation mix (10 µL DNase I stock solution in 70 µL Buffer RDD) at 25 °C for 15 minutes to digest DNA. RNA bound to the silica-membrane in the spin column while other contaminants are efficiently washed away by centrifugation with washing buffers RWT and RPE. Total RNA is then eluted in RNase-free water. RNA amount and quality were assessed using a NanoDrop 2000 spectrophotometer.

2.2.4.3 Reverse transcription

The reverse transcription of total RNA into a complementary DNA (cDNA) was carried out using the SuperScript III Reverse Transcriptase Kit (Invitrogen) according to the manufacturer's instructions. In the first step, the mixture of total RNA, Oligo-dT Primers, Random Hexamers, and dNTPs was initially incubated for 5 minutes at 65 °C in Mastercycler® Gradient and then stored on ice for 1 minute. In the second incubation step, 5 × First-Strand Buffer, dithiothreitol, RNaseOUT Recombinant Ribonuclease Inhibitor, and SuperScript III Reverse Transcriptase were pipetted into the mixture, and cDNA was synthesized in the thermal cycler under the following reaction conditions:

1) 5 minutes, 25 °C

2) 45 minutes, 50 °C

3) 15 minutes, 70 °C

2.2.4.4 Quantitative Real-Time PCR

Quantitative real-time polymerase chain reaction (qRT-PCR) was performed using specific primers and Universal Probe Library (UPL) probes. All measurements were performed on the LightCycler 480 II thermal cycler with 10 ng cDNA was used per reaction mixture in duplicate. The complete reaction mixture (20 µL/well) was

composed as follows:

cDNA (10ng/well)	5 µL
Nuclease-free water	4.4 µL
Forward Primer	0.2 µL
Reverse Primer	0.2 µL
UPL-Probe	0.2 µL
LightCycler 480 Probes Master	10 µL

After an initial denaturation for 10 minutes at 95 °C, the reaction proceeded under the following conditions:

1) Denaturation: 15 seconds: 95 °C
2) Annealing: 30 seconds: 50 °C
3) Elongation: 15 seconds: 72 °C

   30 seconds: 40 °C

The quantitative real-time PCR was carried out in duplicate. The relative mRNA expression of the target gene was normalized to the expression of the reference genes Glyceraldehyde-phosphate dehydrogenase (GAPDH) and TATA Box Binding Protein (TBP). The crossing point (Cp) value corresponds to the cycle at which there is a significant detectable increase in fluorescence was measured and further calculated by the LightCycler® 480 Relative Quantification software.

2.2.4.5 Quantification of miRNA expression

For quantifying miRNA expression, total RNA that was isolated by miRNeasy Mini kit was reversely transcribed using TaqMan® MicroRNA Reverse Transcription Kit. U47 and cel-miR-39-3p were chosen as the internal control for cellular RNA and the spike-in control for exosome RNA, respectively. Each reaction mixture contained 3 µL total RNA (2 ng/µL) and the master mix for a total volume of 6 µL consisted of:

dNTP (100 mM)	0.09 µL
MultiScribe Reverse Transcriptase (50 U/µL)	0.6 µL
10 × Reverse Transcription Buffer	0.9 µL
Rnase Inhibitor (20 U/µL)	0.114 µL
Nuclease-free water	0.696 µL
5 × RT-Primer for miR-125a	1.8 µL
5 × RT-Primer U47/cel-miR-39-3p	1.8 µL

After 5 minutes incubation on ice, the samples were transcribed into cDNA in three steps:

1) 30 minutes, 16 °C
2) 30 minutes, 42 °C
3) 5 minutes, 85 °C

The cDNA was then amplified in duplicates using TaqMan® MicroRNA Assay in

LightCycler 480 II thermal cycler. A reaction mixture (20 µL) was composed as follows:

cDNA	5 µL
TaqMan miR-125a/U47/cel-miR-39-3p assay	1 µL
LightCycler 480 Probes Master	10 µL
Nuclease-free water	4 µL

The reaction conditions:

1) 10 minutes, 95 °C
2) 50 cycles: 15 seconds, 95 °C
   60 seconds, 60 °C
3) 30 seconds, 40 °C

2.2.5 Cloning of reporter constructs of ACTN4, RAC2, and PTPN1

The 3'UTR of ACTN4, RAC2, and PTPN1 were cloned into the Multiple Cloning Site (MCS) of the psiCHECK™-2 vector to determine direct miR-125a interactions with the target genes through co-transfection experiments and Dual-Glo Luciferase Assay. The 3'UTRs of target genes were first amplified by PCR from genomic DNA. The PCR products were ligated into StrataClone Blunt PCR Cloning Vector pSC-B-amp/kan and finally subcloned into the NotI-HF and XhoI restriction sites of the psiCHECK™-2 vector.

2.2.5.1 Construct StrataClone PCR cloning vector

The 3'UTRs of the target genes were amplified from genomic DNA by PCR. Blunt-ended PCR products were ligated into the StrataClone Blunt PCR Cloning Vector pSC-B-amp/kan by topoisomerase I mediated strand ligation.

Genomic DNA was isolated from the blood of healthy persons using the QIAamp DNA Mini Kit according to the manufacturer's instructions. The PCR reaction mixture of template DNA was composed as follows:

Template DNA (100ng/μL)	0.5 μL
10 × *PfuUltra* II Reaction Buffer	2.5 μL
dNTP mix (25 mM each dNTP)	0.25 μL
Primer Forward	0.5 μL
Primer Reverse	0.5 μL
PfuUltra II fusion HS DNA polymerase	0.5 μL
Nuclease-free water	20.25 μL

The mixture was prepared 8 times to get optimal primer hybridization temperatures by means of temperature gradients (with primer TM minus 5 °C as the middle temperature). Using specific ACTN4, RAC2, or PTPN1 forward and reverse primers, template DNA was amplified in three steps using PCR:

1) 2 minutes: 95 °C

2) 30 cycles: 20 seconds: 95 °C

20 seconds: (Primer TM) – 5 °C

30 seconds: 72 °C

3) 3 minutes: 72 °C

PCR product was analyzed by agarose gel electrophoresis in the Sub-Cell GT electrophoresis system. The PCR product was mixed with a 6x loading buffer and separated in a 1% agarose gel at 120V for 60 minutes. The bands were then detected under UV light and the PCR product, which was amplified with the optimal primer hybridization temperature, could be recognized by the clearly visible band and was used for the subsequent ligation into the StrataClone Blunt vector arms. The expected fragment size of ACTN4 was 808 bp, RAC2 was 685 bp, PTPN1 was 501 bp.

The ligation reaction mixture was prepared by combining the following components in order:

StrataClone Blunt Cloning Buffer	3 μL
PCR product (5-50 ng)	2 μL
StrataClone Blunt Vector Mix amp/kan	1 μL

The ligation reaction mixture was mixed gently by repeated pipetting, incubated at room temperature for 5 minutes and then stored on ice for later transforming the competent cells.

StrataClone SoloPack competent cells (50 μL) were thawed on ice and carefully mixed with the entire ligation mixture. After incubation on ice for 20 minutes, the transformation mixture was heat-shocked at 42 °C for 45 seconds to permeabilize the

competent cells to absorb the ligated vector. The transformation mixture was incubated on ice for 2 minutes before 250 μL pre-warmed LB medium was added. The competent cells recovered for 1 hour on a horizontal shaker (225 rpm) at 37 °C and then plated on LB agar plates with 100 μg/mL ampicillin and 40 μL of 2% X-gal on each plate. Only colonies successfully transformed with the plasmid could grow due to the ampicillin resistance gene in the vector and white or light blue colonies were picked for plasmid DNA analysis.

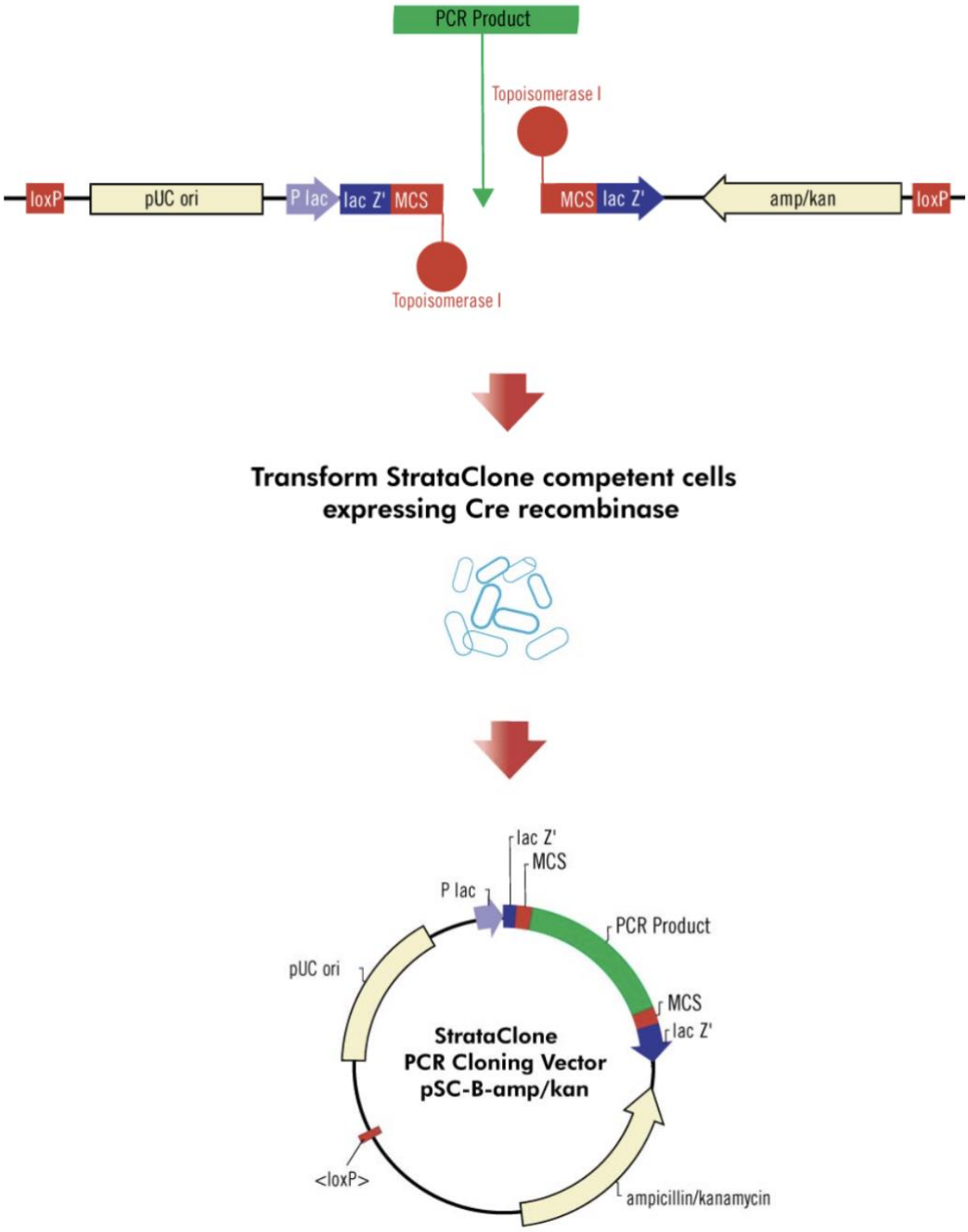

Figure 1　Overview of the StrataClone blunt PCR cloning method

The StrataClone blunt PCR cloning vector contains two blunt-ended DNA arms, blunt-ended PCR products, produced by *PfuUltra* II fusion HS DNA polymerase, are efficiently ligated to these arms by topoisomerase I-mediated strand ligation. The ligation products then transformed into competent cells which transiently expressed Cre

recombinase to recombinant the vector loxP sites and created a circular DNA molecule. These circular DNA plasmids replicate in cells growing in the ampicillin-containing medium and produces lac Z′α (β-galactosidase) for blue-white screening on X-gal coated agar plates.

Source: Agilent.com

2.2.5.2 Restriction digestion and psiCHECK™-2 vector ligation

The restriction digestion of the StrataClone PCR Cloning Vector and psiCHECK™-2 vector was carried out by the same restriction enzymes XhoI and NotI. The cutting pattern of the restriction enzymes creates 5' overhang "sticky ends", which facilitate subsequent ligation. The following reaction mixture was digested for one hour at 37 °C:

DNA	4 μg
10 × NEB CutSmart Buffer	5 μL
100 × Purified BSA	0.5 μL
XhoI (20 U/μL)	0.5 μL
NotI (20 U/μL)	0.5 μL
Nuclease-free water	make up the total volume to 50 μL

After restriction enzyme digestion, the cut-out products were separated by agarose gel electrophoresis. The desired DNA fragment was cut out of the gel under UV light and purified using the Monarch DNA Gel Extraction Kit. Four volumes of Gel Dissolving Buffer were added to the gel slice and incubated at 50 °C until the gel slice was completely dissolved, followed by silica-membrane purification of DNA fragments.

Dephosphorylation of the purified psiCHECK™-2 vector was carried out by Rapid DNA Dephos & Ligation Kit. The reaction mixture was composed as follows:

psiCHECK™-2 vector DNA	1 μg
10 × rAPid Alkaline Phosphatase Buffer	2 μL
rAPid Alkaline Phosphatase	1 μL (1 U)
Nuclease-free water	make up the total volume to 20 μL

The reaction mixture was incubated at 37 °C for 10 minutes, followed by 75 °C for 2 minutes in order to inactivate the phosphatase. DNA insert fragment was then ligated into the psiCHECK™-2 vector using T4 DNA ligase, the reaction took 5 minutes at room temperature:

Vector: Insert	1:3 (Molar ratio)
5 × DNA Dilution Buffer	2 μL
Nuclease-free water	make up the above volume to 10 μL
2 × T4 DNA Ligation Buffer	10 μL
T4 DNA Ligase	1 μL

Ligated psiCHECK™-2 vector was transformed to NEB 10-beta Competent E. coli. After incubation on ice for 30 minutes, the transformation mixture was heat-shocked at 42 °C for 30 seconds and again incubated on ice for 5 minutes. Next, 950 μL pre-warmed SOC medium was added to obtain maximal transformation efficiency. The competent E. coli recovered for 1 hour on a horizontal shaker (225 rpm) at 37 °C and

then plated on the ampicillin-containing agar plate. Only colonies successfully transformed with the plasmid could grow due to the ampicillin resistance gene in the psiCHECK™-2 vector.

The plasmids were isolated using the PureYield Plasmid Midiprep Systems. The sequence of the 3'UTR in the psiCHECK™-2 vector was detected by Sanger sequencing (MWG Eurofins). The result was checked for consistency with the target sequence using PubMed Basic Local Alignment Search Tool (BLAST).

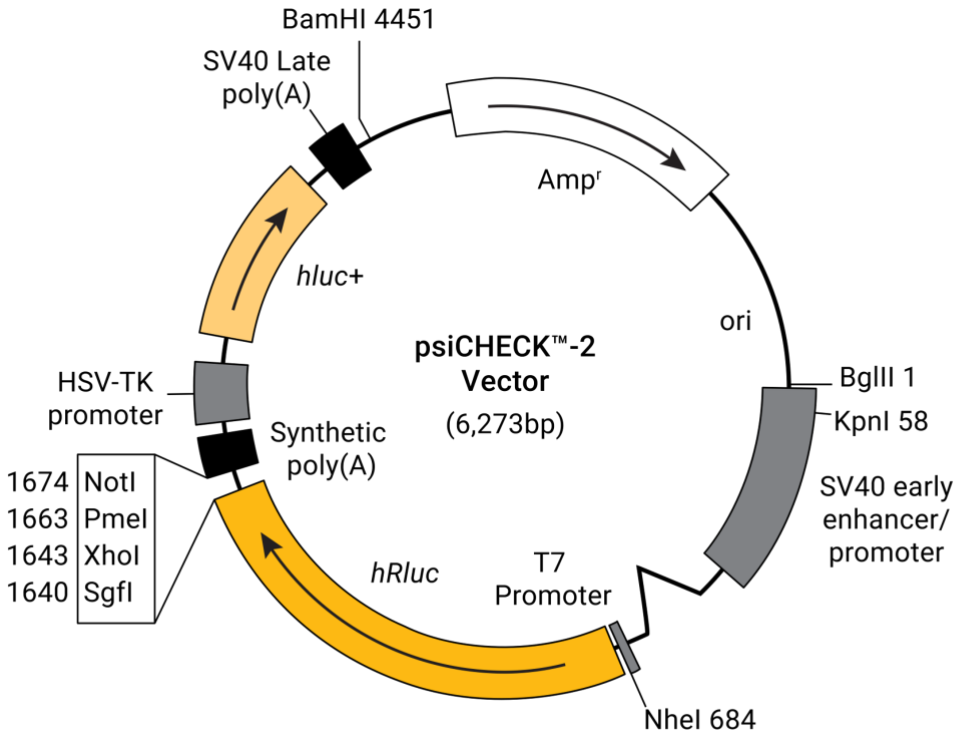

Figure 2 psiCHECK™-2 vector

The multiple cloning site (MCS) of the vector is located at the 3' end of the Renilla luciferase gene (hRluc), containing restriction enzyme sites NotI, PmeI, XhoI, and SgfI. The vector was cut at NotI and XhoI and ligated with 3'UTR of the target gene to be examined. Binding with simultaneously transfected miR-125a leads to reduced Renilla luminescence. The constantly expressed firefly luciferase (hluc+) served as control.

Source: Promega GmbH

2.2.5.3 Mutagenesis of miR-125a binding sites

In order to verify the putative binding sites of the miR-125a in the PTPN1 3'UTR, site-directed mutagenesis of the PTPN1-psiCHECK™-2 vector was performed using QuikChange Lightning Multi Site-Directed Mutagenesis Kit. The reaction mixture was composed as follows:

Plasmid DNA	100 ng
Mutagenesis Primer Forward	0.5 µL
Mutagenesis Primer Reverse	0.5 µL
dNTP Mix	1 µL
QuikSolution Reagent	1.5 µL
10 × Reaction Buffer	5 µL
QuikChange Lightning Enzyme	1 µL
Nuclease-free water	make up the total volume to 50 µL

Mutant strand synthesis reaction took in three steps in thermocycler:

1) 2 minutes: 95 °C
2) 18 cycles: 20 seconds: 95 °C
   10 seconds: 60 °C

30 seconds/kb of plasmid: 68 °C

3) 5 minutes: 68 °C

The amplification products were digested with Dpn I restriction enzyme for 15 minutes at 37 °C. XL10-Gold ultracompetent cells were thawed on ice. 45 µL of cells were mixed with 2 µL β-mercaptoethanol in a prechilled 14 mL tube. Cells were incubated on ice for 10 minutes, swirled gently every 2 minutes. The Dpn I treated amplification products were then again introduced into XL 10-Gold UltraCompetent Cells by means of heat shock transformation. After plasmid isolation, Sanger sequencing was used to confirm the mutation.

2.2.5.4 Plasmid isolation and DNA gel extraction

The plasmid isolation from E. coli was carried out using the PeqGold Plasmid Miniprep Kit I (for smaller yield) or the Pure Yield™ Plasmid Midiprep System depending on the required DNA yield. For this purpose, 3 mL of the LB supernatant with an individually picked E. coli colony was required for the mini-preparation, while 100 mL for midi-preparation. Colonies on LB agar plates were picked to further proliferation in the corresponding volume of LB medium with 100 µg/mL Ampicillin for 16 hours at 37°C in a shaker. The alkaline solution was used in both systems to burst bacteria. The mixture was centrifuged at high speed and then the supernatant was transferred to a column containing silica membrane where plasmid DNA adheres. Plasmid DNA was finally eluted from the column membrane with nuclease-free water. DNA amount and quality assessed by NanoDrop 2000 spectrophotometer.

2.2.6 Reporter gene assays

2.2.6.1 Transient co-transfection of HEK-293 cells

HEK-293 cells were transfected to perform a Dual-Luciferase reporter gene assay. For this, 100,000 HEK-293 cells were resuspended in Neon™ resuspension buffer R and well mixed with 50 nM pre-miR-125a or pre-miR negative control and 1 µg psiCHECK™-2 plasmid containing the cloned 3′UTR of the target gene (wild type or in mutated type). Co-transfection was done in a 10 µL Neon™ transfection tip at 1150 volts (20 ms, 2 pulses), followed by 40 hours of incubation in DMEM medium without antibiotic at 37 °C.

2.2.6.2 Dual-Glo luciferase reporter gene assay

Dual-Glo Luciferase Reporter Gene Assay was carried out according to the manufacturer's protocol. The psiCHECK™-2 vector constantly expresses a gene for the firefly luciferase and serves as an internal control to normalize the transfection efficiency. The 3'UTR of the target genes was subcloned into the Multiple Cloning Site (MCS) of the psiCHECK™-2 vector at the 3' end of the Renilla luciferase gene. The binding of miR-125a to the subcloned target gene 3'-UTR leads to a degradation of the mRNA and a corresponding decrease in Renilla luciferase activity. This made it possible to quantify the direct miR-125a regulation of the target genes.

Forty hours after transfection, HEK-293 cells were harvested, washed with PBS, and resuspended in 20 µL DMEM medium. Cell suspension (15 µL) and an equal volume of Dual-Glo Luciferase reagents were added into a 96-well plate and mixed well in dark. Firefly luciferase (control luciferase) was activated during the following 10 minutes incubation. Luminescence was quantified in the FilterMax F3 MultiMode Microplate Reader. Then the samples were mixed with 15 µL Dual-Glo Stop and Glo

Reagent (in a ratio of 1:100), which reduced the firefly luciferase signal and contained the substrate for Renilla luciferase. After another 10 minutes of reaction in the dark, the luminescence of the Renilla luciferase was measured and the relative luciferase activity was determined by normalizing to the firefly luciferase activity. This determined ratio indicated the regulation of the target mRNA by miR-125a. All experiments were performed in triplicates.

2.2.7 Western Blot

2.2.7.1 Protein extraction and determination

Cell culture medium was discarded, and HUVEC were washed by ice-cold PBS. HUVEC were lysed in RIPA Lysis and Extraction Buffer containing 1% protease and phosphatase inhibitors. Adherent cells were scraped using a cold plastic cell scraper and the cell suspension was gently collected into a pre-cooled microcentrifuge tube. After sonication 3 times for 30 seconds in an ultrasonic water bath, the tubes were spun at 16,000 × g for 10 minutes in a 4 °C precooled centrifuge. The supernatant was transferred to a fresh tube on ice. Protein concentration was determined using Pierce bicinchoninic acid (BCA) Protein Assay Kit. The BSA standard curve was generated using a four-parameter logistic curve involving a set of six standard points (BSA standards concentration: 0, 0.125, 0.25, 0.5, 1 and 2 mg/mL). BCA reagent A and reagent B were mixed in a ratio of 50:1 to prepare BCA working reagent. Then 10 µL BSA standards or protein samples were placed in a transparent flat-bottom 96-well plate in duplicate and 200 µL of the BCA working reagent was added. The 96-well plate was then incubated in the dark at 37 °C for 30 minutes before the protein concentration was determined at 560 nm by FilterMax F3 MultiMode Microplate Reader.

2.2.7.2 SDS-PAGE gel electrophoresis and membrane transfer

Protein samples were mixed with a laemmli sample buffer and boiled at 95°C for 5 minutes for denaturation. Equal amounts of protein were added into the wells of a mini sodium dodecyl sulfate-polyacrylamide gel electrophoresis (SDS-PAGE) gel, along with 5 μL PageRuler protein ladder. The SDS-PAGE gel consisted of a 4% stacking gel and a 12% separating gel. Electrophoresis was carried out in the 1 × SDS running buffer at 100 V for two hours. When an electric field was applied, the protein migrated to the positively charged anode at different speeds based on their molecular weight. The gel with the separated proteins was then placed in TBST for 5 minutes. The Transfer Pack was placed into the cassette of the Trans-Blot® Turbo Blotting System with gel assembled in between and blotted at 1.3 A, 25 V for 10 minutes. The membrane was incubated in methanol for 10 seconds after the blot.

2.2.7.3 Immunodetection

Nonspecific binding was blocked with 5% non-fat milk or 5% BSA (for Phospho-VE-Cadherin antibody) in TBST for 1 hour. Primary antibodies for α-actinin-4 (1:200), Claudin-5 (1:500), Ets-1 (1:100), PP1α (1:200), PTP1B (1:1000), Rac-2 (1:100), and VE-Cadherin (1:1000) were diluted in TBST with 5% non-fat milk, Phospho-VE-Cadherin antibody (Tyr658) was diluted in TBST with 5% BSA. The membrane was incubated in the primary antibody solution at 4 °C overnight. Before and after incubation in the corresponding HRP-conjugated secondary antibody (1:3000) solution, the blot was washed 3 times for 5 minutes each with TBST. Western ECL Substrates mixture was applied to the blot, and the chemiluminescent signals were captured using a CCD camera-based imager and displayed via Wasabi imaging software. The intensity of the bands obtained was quantified using ImageJ.

β-Actin mouse mAb (1:1000) served as the loading control. After the target protein was

developed, the membrane was first washed with TBST, then incubated twice for 10 minutes with the stripping buffer and then washed again with TBST. The bands were developed by means of chemiluminescence according to the steps mentioned above.

2.2.8 Immunofluorescence

To enhance endothelial cell adhesion, the µ-Slides $I^{0.4}$ Luer for cell culture were pre-coated. The slides were incubated with 50 µg/mL Poly-L-Lysine for 20 minutes, 0.5% glutaraldehyde for 15 minutes, and 0.2% gelatine for 10 minutes in turn and washed with HBSS three times after each coating step. Then the slides were incubated with ECGM culture medium at 37 °C overnight. Before cell seeding, the slides were washed five times with the antibiotic-free ECGM culture medium.

Pre-miR-125a and pre-miR negative control transfected HUVECs (1.5×10^5 cells/slide) were seeded in slide, cultured at 37 °C and 5% CO2 in the antibiotics-free medium for 48 hours. Cells were fixed with 4% paraformaldehyde in PBS for 10 minutes at room temperature. Once fixed, the cells were rinsed three times with PBS and subsequently permeabilized with 0.1% Triton X-100 in PBS for 10 minutes. Cells were incubated in 5% normal goat serum plus 5% BSA in PBS for 1 hour at room temperature for preventing non-specific binding of antibodies or other reagents to the cells. Primary antibody diluted in PBS with 2% BSA (VE-Cadherin, 1:100; claudin-5, 1:100) was incubated with cells overnight at 4°C. Slides were washed three times with PBS for 5 minutes each and stained with fluorochrome-conjugated secondary antibodies (Alexa Fluor 488, 1: 400) and To-Pro-3 (1:1000) in PBS with 2% BSA for 2 hours at room temperature in dark. After rinsing three times in PBS for 5 minutes each in dark, slides were mounted with a drop of mounting medium.

Samples were observed under LEICA-TCS SP5 confocal microscope and images were acquired using the Leica application suite AF software, version 2.7.

2.2.9 Electric cell-substrate impedance sensing (ECIS®)

ECIS® 8W10E+ PET arrays were used for ECIS® measurements, each containing 8 wells with two sets of 20 electrodes mounted on interdigitated fingers to provide measurements of cells upon a total of 40 electrodes. ECIS 8W10E+ PET arrays were pre-coated with 0.2% gelatin (dissolved in sterile aqua) for 1 hour at 37 °C. Then, the arrays were washed three times with aqua and incubated with Endothelial Cell Basal Medium overnight in the incubator. The medium was changed to ECGM culture medium without antibiotics 1 hour before seeding the cells. Before the arrays to be used for an experiment were loaded into the ECIS® Station 16W of the ECIS® Z system. Electrode stabilization was applied to clean the gold electrode surfaces and reduce unwanted drift in impedance during an experimental run. Multiple Freq./Time (MFT) mode was used for measurement and the base value when the cells are not inoculated was recorded. Transfected HUVEC were inoculated at 100,000 cells/well. After 48 hours of incubation, cells were stimulated with TNF (25 ng/mL) for 24 hours. For analysis of barrier function, the area under the curve (AUC) of normalized impedance values at 4,000 Hz was calculated.

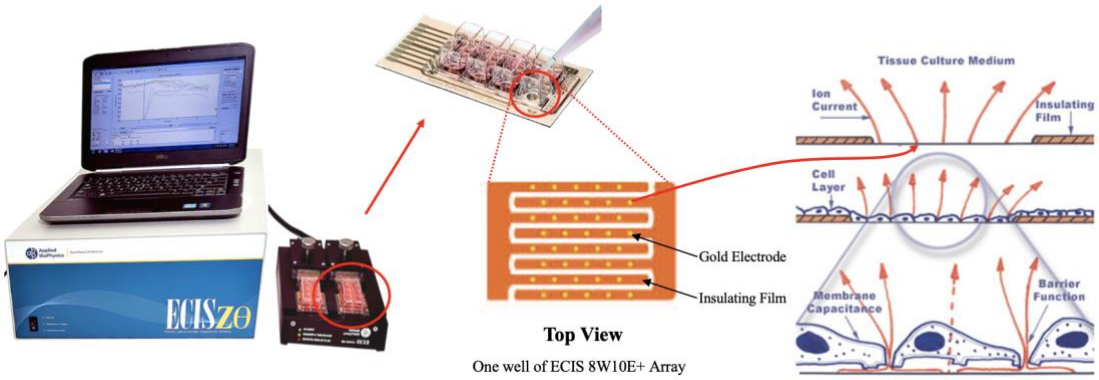

Figure 3 Electric cell-substrate impedance sensing

ECIS® is a real-time impedance-based cell monitoring system. ECIS® system-generated alternating current with a given frequency and HUVEC monolayer formed on the gold electrodes act as insulators increasing the impedance. The impedance was calculated from the corresponding changes in voltage between working electrodes and counter electrodes, which reflect cell barrier function.

Source: modified from biophysics.com

2.2.10 FITC-BSA passage (permeability assay)

Endothelial permeability was assessed by measuring the passage of Fluorescein isothiocyanate conjugated bovine serum albumin (FITC-BSA) across confluent HUVEC monolayers. Transfected HUVEC were cultured in 24 well ThinCert™ translucent cell culture inserts (pore size 0.4 μm) placed in a 24-well plate with 200 μL ECGM medium in the upper compartment and 800 μL ECGM medium in the lower compartment. After 48 hours of incubation, the formation of the HUVEC monolayer was checked by transferring cell culture inserts into empty wells and the culture medium in the upper compartment should not leak out of the inserts. HUVEC were stimulated with TNF (25 ng/mL) for 24 hours. For permeability analysis, the medium in the lower compartment was then changed to 800 μL Endothelial Cell Basal Medium without any supplement and 10 μL of FITC-BSA (10 mg/ mL) was added into the upper compartment of each insert. After 30 minutes, 50 μL medium from the lower compartment was collected into a Nunc 96-well black plate as a duplicate. Fluorescence intensity was measured by FilterMax F3 MultiMode Microplate Reader using Fluorescence Intensity (FL) read mode with an excitation wavelength of 485 nm and an emission wavelength of 535 nm.

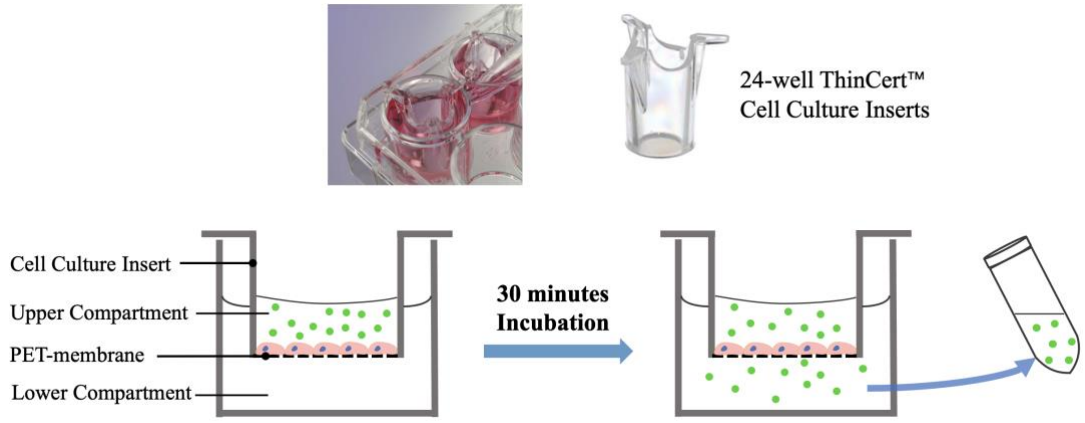

Figure 4 Permeability assay

HUVEC were cultured in 24-well ThinCert™ translucent cell culture inserts placed in 24-well culture plates. After transfection, HUVEC were incubated for 48 hours and then stimulated with 25 ng/ml TNF for 24 hours. Subsequently, 10 µg FITC-BSA was added to the upper compartment of each insert and the medium of bottom wells was collected after 30 minutes for measurement.

Source: modified from Greiner Bio-One GmbH

2.2.11 Bioinformatics analysis and statistics

Analysis and interpretation of transcriptomic signatures of pathways found in NGS-based RNA-Seq were performed by Gene Set Enrichment Analysis (https://www.gsea-msigdb.org/gsea/index.jsp). Analysis of potential miR-125a mRNA binding sites on selected target genes were determined using the prediction programs TargetScanHuman 7.2 (http://www.targetscan.org) and miRIAD (http://bmi.ana.med.uni-muenchen.de/miriad/). The DNA sequence of the 3'UTRs was determined using PubMed (http://www.ncbi.nlm.nih.gov/pubmed) and 3'UTR primers were created using Primer3Plus (https://primer3plus.com/). The restriction enzyme sites were assessed with NEBcutter V2.0 (http://nc2.neb.com/NEBcutter2/). For RNA-Seq results, the

differential gene expression analysis was carried out with non-corrected p-value < 0.05 and fold change +2 to -2 to identify potential targets. For Gene Set Enrichment Analysis, pathways with false discovery rate corrected p-values < 0.01 were seen as significant.

If not stated otherwise, the values are shown to represent the means ± standard error of the mean (SEM). The repetitions of the experiments are indicated as n; at least triplicates were carried out. Statistical analyses were performed using GraphPad Prism 7. p-values were calculated using student's t-test or paired t-test for all data with normal distribution and Wilcoxon signed-rank test otherwise. p-values below 0.05 were considered statistically significant (* $p < 0.05$; ** $p < 0.01$; *** $p < 0.001$).

3 Results

3.1 The expression of miR-125a in endothelial cells increases in the inflammatory microenvironment

In the process of systemic inflammation, endothelial barrier dysfunction is a critical factor in inducing tissue edema and disease progression. Endothelial cells encounter and respond to insults in the circulation and simultaneously being a target and an amplifier of inflammation. In highly inflammatory disorders such as sepsis and stroke, circulating miR-125a in blood samples of patients is elevated, and correlated with the severity of the disease[87]. Since the main source of circulating miR-125a remains unknown, we first investigated whether the expression of endothelial miR-125a could be induced by inflammatory mediators and consecutively be released through extracellular vesicles.

HUVEC were incubated with the pro-inflammatory cytokines tumor necrosis factor (TNF) and interferon-gamma (IFN-γ). Total RNA was isolated from cells and cell culture supernatant, TaqMan® MicroRNA Assay was used to quantify miR-125a expression. After stimulation, the intracellular expression of miR-125a increased by 68.9% ± 20.7% (n = 6, $p < 0.05$, Fig. 5A). Extracellular vesicles isolated from cell culture supernatant showed that miR-125a expression was upregulated by + 84.1% ± 21.6% (n = 6, $p < 0.01$, Fig. 5B).

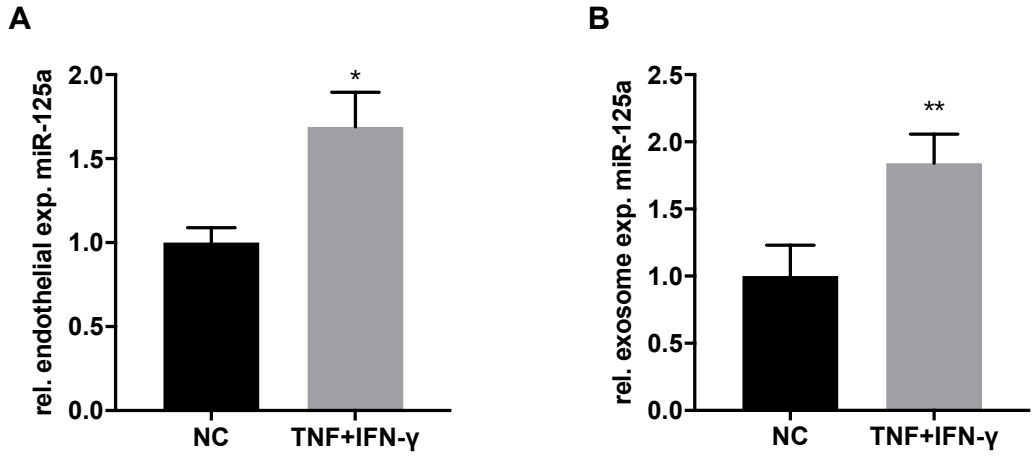

Figure 5 Endothelial miR-125a expression increases upon stimulation with inflammatory cytokines

(A) After 4 hours of 25 ng/mL TNF and 50 ng/mL IFN-γ treatment, the normalized endothelial miR-125a level increased. Endogenous reference: U47. Rel. = relative; exp. = expression; NC = negative control; * $p < 0.05$.

(B) Endothelial exosome miR-125a expression increased after cytokine treatment with 25ng/ml TNF and 50 ng/ml IFN-γ for 4 hours. The values correspond to the miR-125a level in the exosome of stimulated relative to unstimulated cells. Spike-in control: cel-miR-39-3p. Rel. = relative; exp. = expression; NC = negative control; ** $p < 0.01$.

The circulatory system dysfunction, especially microcirculatory perfusion alteration leads to insufficient tissue perfusion and oxygenation, which is frequently observed in the state of systemic inflammation. Next, endothelial cells were stimulated with TNF under hypoxic conditions at 5% O_2. Intracellular induction of miR-125a was increased by 19.9% ± 3.2%, (n = 6, $p < 0.01$, Fig. 6A). The expression of extracellular vesicles miR-125a increased by 103.1% ± 16.8%, (n = 6, $p < 0.01$, Fig. 6B). These results

indicate that inflammation can induce the expression and release of miR-125a in endothelial cells.

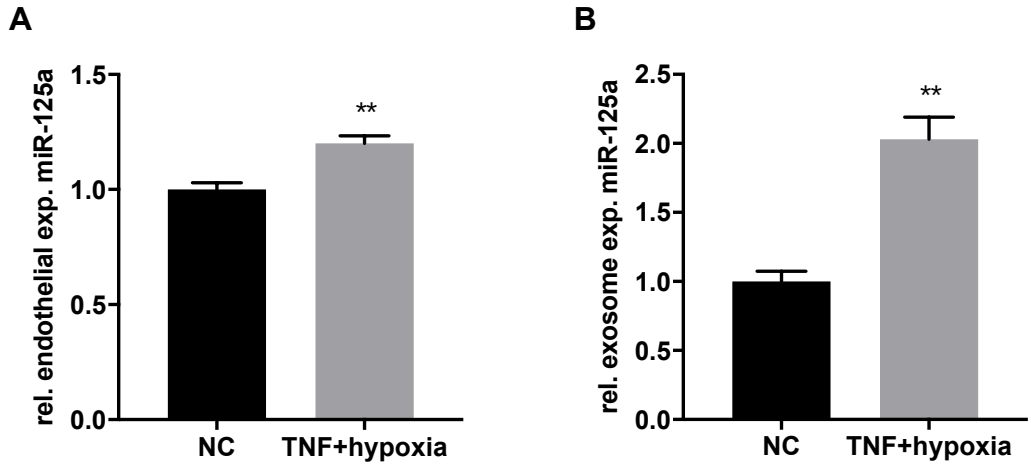

Figure 6 Expression and release of miR-125a increase in endothelial cells stimulated by TNF in a hypoxic environment

(A) Intracellular relative miR-125a levels after stimulation with 25 ng/ml TNF under hypoxic conditions of 5% O_2 and 40 mmHg CO_2 for 24 hours. Endogenous reference: U47. Rel. = relative; exp. = expression; NC = negative control. Mean ± SEM; ** $p < 0.01$.

(B) The level of miR-125a in exosome isolated from cell culture supernatant after stimulation with 25 ng/ml TNF under hypoxic conditions of 5% O_2 and 40 mmHg CO_2 for 24 hours. Spike-in control: cel-miR-39-3p. Rel. = relative; exp. = expression; NC = negative control. Mean ± SEM; ** $p < 0.01$.

3.2 Overexpression of miR-125a alters pathways crucial for endothelial barrier integrity

Since endothelial miR-125a expression was upregulated after inflammatory stimulation, miR-125a may be involved in the regulation of endothelial dysfunction

during inflammation. miRNAs act in functional networks, where a single miRNA is able to regulate multiple target genes, and in turn, one protein-coding mRNA could be regulated by several different miRNAs. Therefore, miRNAs suppress transcripts in the interactome network, thereby simultaneously regulating related signal cascades.

The transcriptome of HUVEC overexpressing miR-125a was analyzed using Next Generation Sequencing (NGS). We combined pathway analysis with in silico target prediction to identify direct targets of miR-125a that possibly regulating endothelial permeability. Five candidate targets of miR-125a that are involved in pathways regulating cell adhesion and cellular junctions as well as contain miR-125a binding sites in their 3' untranslated region (3'UTR) were extracted: Actinin Alpha 4 (ACTN4), Rac Family Small GTPase 2 (RAC2), Protein Tyrosine Phosphatase Non-Receptor Type 1 (PTPN1), Protein Phosphatase 1 Catalytic Subunit Alpha (PPP1CA), and ETS proto-oncogene 1 (ETS-1).

In vitro experimental validation determined that overexpression of miR-125a by electroporation with pre-miR-125a in HUVEC results in a significant reduction of mRNA (Fig. 7A) and protein (Fig. 7B) levels of all these potential targets.

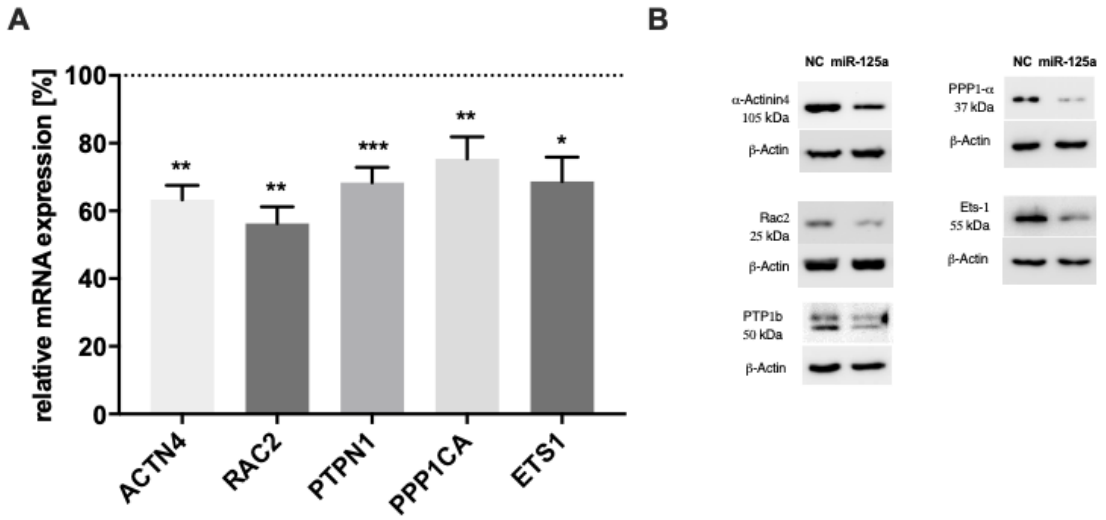

Figure 7 Overexpression of miR-125a inhibits barrier function gene expression profile in endothelial cells

(A) HUVEC were transfected with miR-125a or pre-miR negative control (NC; dashed line) and stimulated with 25 ng/mL TNF for 6 hours. Relative mRNA levels of ACTN4, RAC2, PTPN1, PPP1CA, and ETS-1 were determined in the isolated RNA from HUVEC by qRT-PCR. ACTN4: - 36.7% ± 4.2%, n = 6, $p < 0.01$; RAC2: - 43.7% ± 4.9%, n = 6, $p < 0.01$; PTPN1: - 31.6% ± 4.5%, n = 7, $p < 0.001$; PPP1CA: - 24.6% ± 6.5%, n = 8, $p < 0.01$; ETS1: - 31.3% ± 7.2%, n = 8, $p < 0.05$. Mean ± SEM; * $p < 0.05$; ** $p < 0.01$; *** $p < 0.001$.

(B) Protein expression of ACTN4, RAC2, PTPN1, PPP1CA, and ETS-1 in endothelial cells overexpressing miR-125a were determined by Western blot. A representative graph from n = 3 individual experiments is shown, β-actin was applied as a loading control. ACTN4: - 39.3% ± 10.7%, n = 3; RAC2: - 38.2% ± 8.1%, n = 3; PTPN1: - 64.6% ± 2.2%, n = 4; PPP1CA: - 54.6% ± 22.4%, n = 4; ETS1: - 68.0% ± 5.2%, n = 4. Mean ± SEM.

CDH5 and CLDN5 are principal junction proteins on the endothelial cell membrane. Cell surface availability of these junction proteins is a crucial part of maintaining endothelial barrier function. With TNF stimulation, the reduction of surface expression of CDH5 (Fig. 8A) and CLDN5 (Fig. 8B) was detected in HUVEC overexpressing miR-125a by immunofluorescent staining. Together, these data suggest that overexpression of miR-125a reduced expression of key components for endothelial barrier function.

A

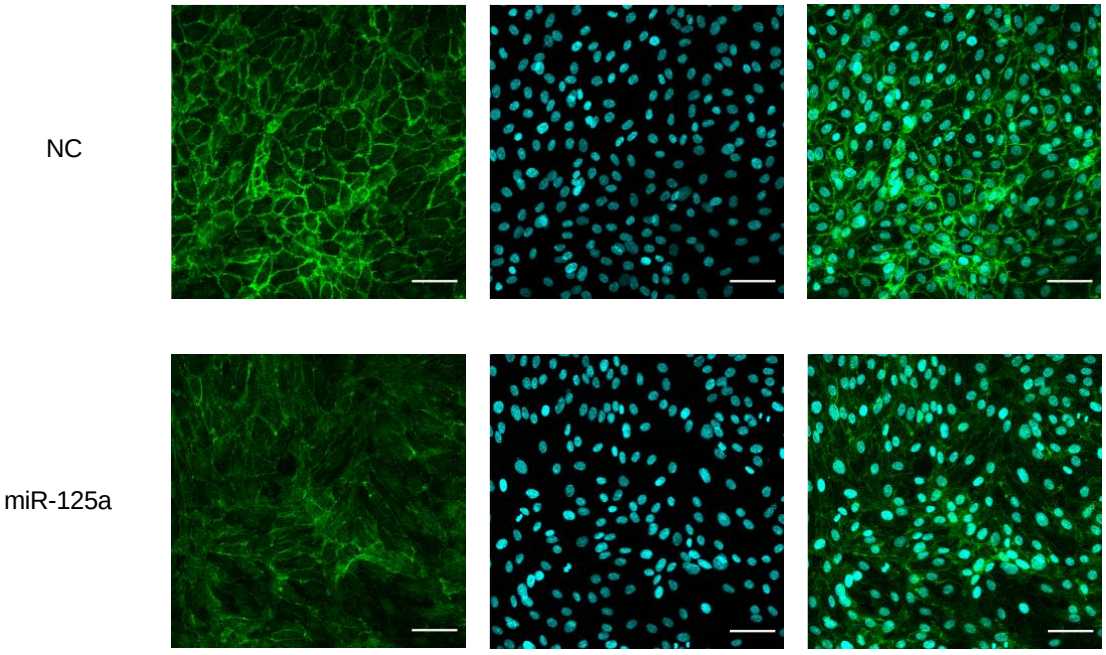
NC
miR-125a
VE-cadherin
To-Pro-3
Merge

B

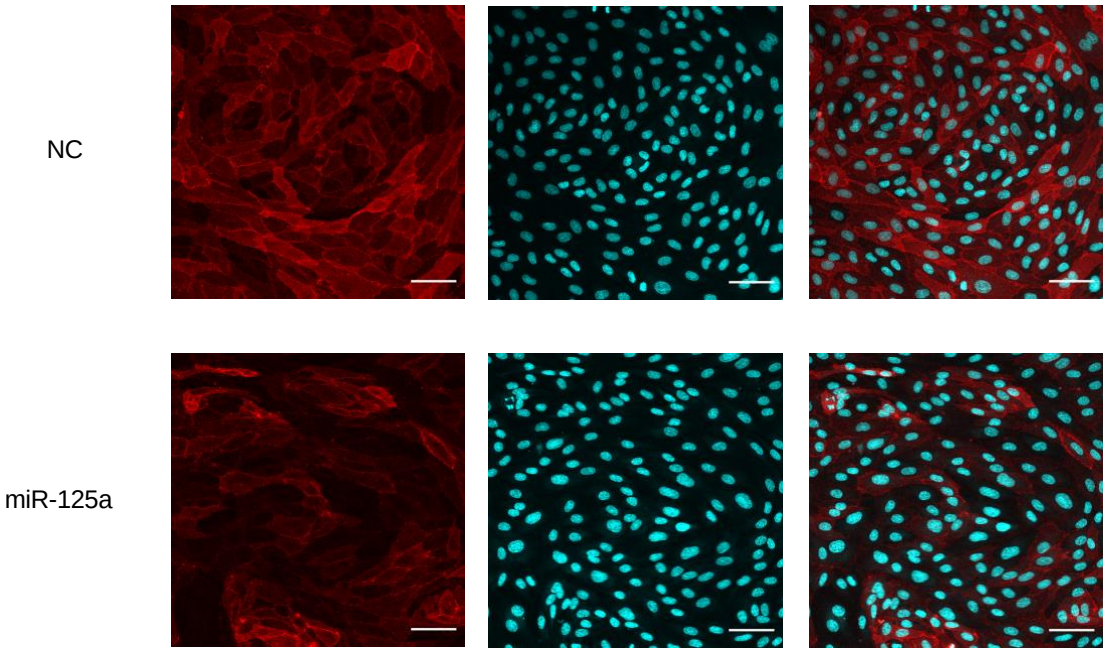
NC
miR-125a
claudin-5
To-Pro-3
Merge

Figure 8 Endothelial cells express less surface CDH5 and CLDN5 after miR-125a transfection and TNF stimulation

(A) Immunofluorescence staining of the adherens junction protein VE-cadherin and the cell nucleus in HUVEC transfected with pre-miR negative control or pre-miR-125a, followed by 6 hours of 25 ng/mL TNF stimulation. Merged images (right): VE-cadherin (green) and nuclear staining with To-Pro-3 (cyan). Representative images of n = 3 to 4 experiments. Scale bars, 60 μm.

(B) HUVEC were either transfected with pre-miR negative control or pre-miR-125a and stimulated with 25 ng/mL TNF for 6 hours. Representative immunofluorescence staining images of n = 3 to 4 experiments were shown. Merged images (right): claudin-5 (red) and nuclear labeled with To-Pro-3 (cyan). Scale bars, 60 μm.

3.3 Overexpression of miR-125a impairs endothelial barrier function

As overexpression of miR-125a alters pathways that are essential for endothelial junctions, the phenotypic effects of miR-125a were then investigated focusing on endothelial barrier integrity. HUVEC were transfected with pre-miR-125a or pre-miR negative control. As indicators of endothelial barrier function, trans-endothelial passage of FITC-albumin and real-time endothelial electric impedance were evaluated.

In fact, overexpression of miR-125a significantly weakened endothelial barrier function, shown by an increase in basal (+ 1.9-fold, n = 6, $p < 0.05$; Fig. 9) and TNF-induced (+ 2.3-fold, n = 6, $p < 0.01$) passage of macromolecules.

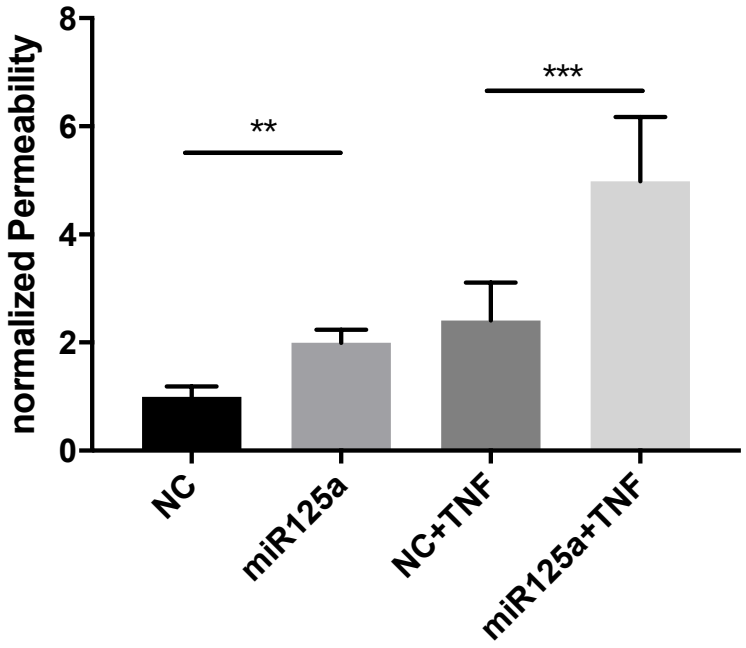

Figure 9 Trans-endothelial passage of FITC-albumin increases in miR-125a transfected HUVEC

HUVEC were transfected with 50 nM pre-miR negative control (NC) or pre-miR-125a. Permeability of FITC-albumin through the endothelial monolayer was measured 72 hours after transfection (including 24 hours of 25 ng/mL TNF stimulation). Permeability of HUVEC monolayer is represented by relative fluorescence intensity of collected medium. Compared with NC, the permeability of HUVEC transfected with pre-miR-125a was increased by 99.7% ± 26.2% (n = 6, $p < 0.01$. After TNF stimulation, permeability of pre-miR-125a transfected HUVEC is increased by 128.0% ± 27.6% (n = 6, $p < 0.01$). Mean ± SEM; ** $p < 0.01$; *** $p < 0.001$.

Permeability assays can only be performed at fixed time points. In order to further verify the change of endothelial cell permeability, the electric impedance of the endothelial monolayer was measured by the ECIS® system in real-time during the

entire experiment. Impairment of the endothelial barrier function results in a decrease in impedance. In HUVEC overexpressing miR-125a, impedance detected at 4,000 Hz decreased (Fig. 10A). For quantitative analysis, the area under the curve (AUC) was calculated (AUC: - 17.1% ± 4.5%, n = 4, $p < 0.01$; Fig. 10B). This indicates that inflammation induced miR-125a impairs endothelial barrier integrity.

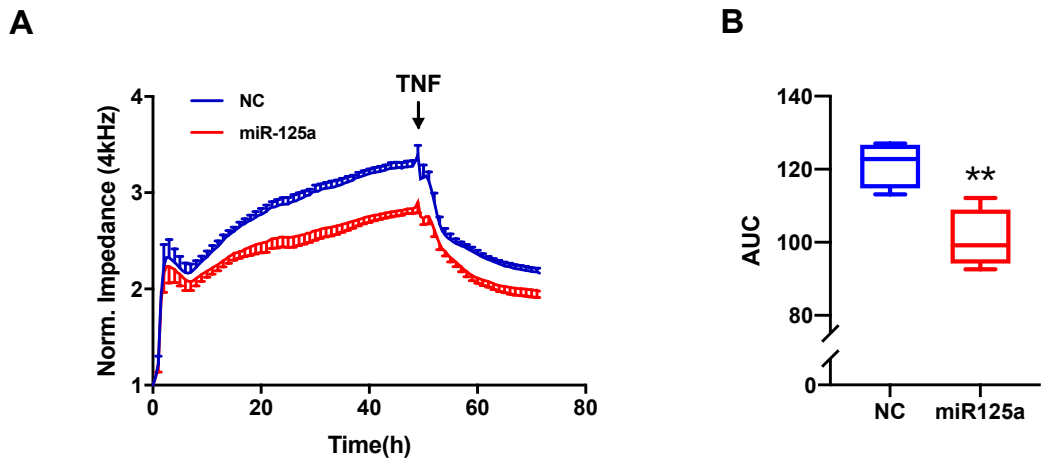

Figure 10 Transfection of HUVEC with miR-125a reduces endothelial electrical impedance

Transfected HUVEC were cultured in ECIS 8W10E+ PET arrays for 48 hours, followed by 24 hours of 25 ng/mL TNF stimulation.

(A) Decreased endothelial electrical impedance was observed in HUVEC transfected with pre-miR-125a compared to pre-miR negative control (NC) under basal and stimulated conditions. Impedance was recorded over time at 4,000 Hz and normalized to the reference impedance measured before cell inoculation.

(B) Area under the curve (AUC) was calculated from (A) for quantitative analysis. Mean ± SEM; n = 4; ** $p < 0.01$.

3.4 PTPN1, PPP1CA and ETS1 are direct targets of miR-125a

In order to verify whether the putative targets identified by Next Generation Sequencing and in-silico target prediction are indeed directly regulated by miR-125a, that is, the miR-125a seed region binds to the 3'UTR of the target gene, reporter gene assays were performed using psiCHECK™-2 vector ligated with respective 3'UTR of the target gene. PPP1CA and ETS1 were previously confirmed as direct targets of miR-125a[94, 95], while the interaction between 3'UTR of ACTN4, RAC2, PTPN1 and miR-125a need to be determined.

HEK-293 cells were co-transfected with the respective reporter vectors and miR-125a to perform a Dual Luciferase reporter gene assay. Repression of the target gene by miR-125a was manifested as a decrease in relative luciferase activity. Co-transfection of miR-125a and wild-type PTPN1 (WT PTPN1) plasmid confirmed repression of PTPN1 by 16.3% ($n = 6$, $p < 0.001$; Fig. 11). After the miR-125a binding site in PTPN1-3'UTR was mutated, the regulatory effect could be eliminated.

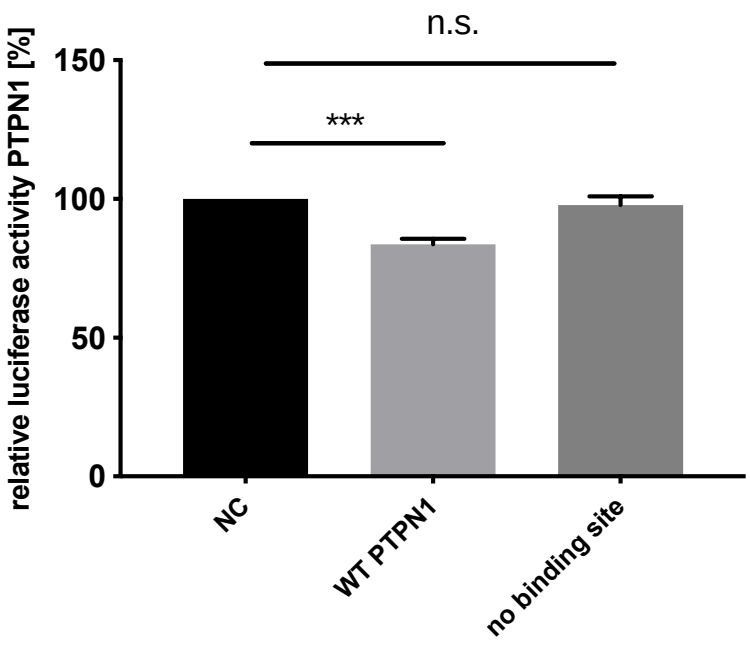

Figure 11 Target validation identifies PTPN1 as a direct target gene of miR-125a

The wild-type PTPN1-3'UTR or miR-125a binding site mutated PTPN1-3'UTR was cloned into the psiCHECK™-2 vector and co-transfected with pre-miR-125a or pre-miR negative control (NC) into HEK-293 cells. Transfection with miR-125a resulted in binding to the 3'UTR of wild-type PTPN1 and the degradation of the mRNA, which then reduced the Renilla luciferase activity. The values correspond to Renilla / Firefly luciferase activity relative to the transfection of NC. A ratio < 100% suggests a direct miR-mRNA interaction. All Luciferase experiments were performed in triplicates. Mean ± SEM; ***p < 0.001. n.s. = not significant.

However, after co-transfection with miR-125a, the luciferase activity of the psiCHECK-2 vector fused with 3'UTR of ACTN4 and RAC2 did not change (Fig. 12). Together, PTPN1, PPP1CA, and ETS-1 are direct targets of miR-125a, while ACTN4, and RAC2 represent indirect targets.

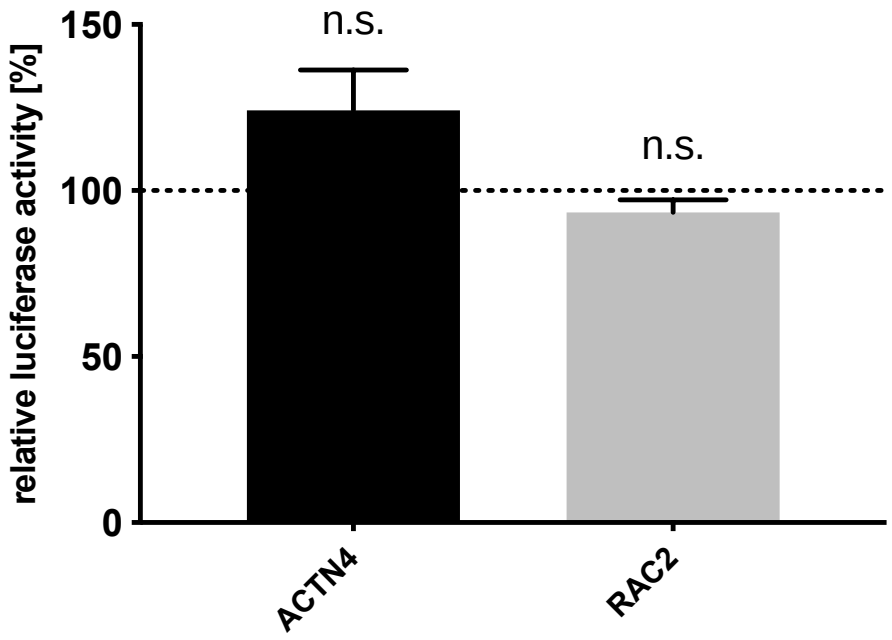

Figure 12 ACTN4 and RAC2 are indirect targets of miR-125a

The 3'UTR of ACTN4 and RAC2 was cloned into the psiCHECK™-2 vector, respectively. Constructed vectors with pre-miR-125a or pre-miR negative control (NC) were co-transfected into HEK-293 cells. The relative luciferase activity is shown. All Luciferase experiments were performed in triplicates. Mean ± SEM; n.s. = not significant.

3.5 CLDN5 is regulated by miR-125a and reciprocally regulates the expression of CDH5

Endothelial cells express cell type-specific adhesion proteins such as VE-cadherin at adherens junctions (AJs) and claudin-5 at tight junctions (TJs), which are functionally linked and play a critical role in endothelial barrier formation. Next Generation Sequencing showed a significant downregulation of CLDN5 level in miR-125a overexpressing HUVEC. For experimental validation, HUVEC were transfected by

electroporation with pre-miR-125a or miR-125a negative control. There was a clear reduction of CLDN5 mRNA level after miR-125a overexpression quantified by qRT-PCR (mRNA: - 64.5% ± 1.5%; n = 4; $p < 0.01$; Fig. 13A). Protein expression of CLDN5 after transfection was then determined by Western blot analysis (protein: - 80.2% ± 7.7%; n = 4; Fig. 13B).

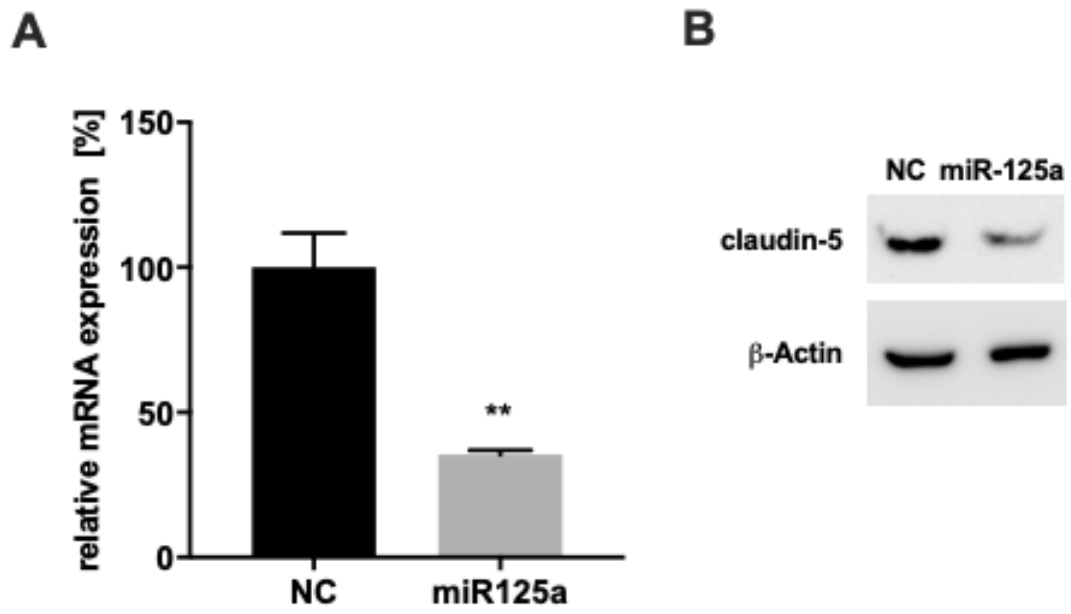

Figure 13 CLDN5 mRNA and protein expression in HUVEC is downregulated by miR-125a

HUVEC were transfected with pre-miR negative control (NC) or pre-miR-125a and stimulated with 25 ng/mL TNF for 6 hours. Cells were harvested 48 hours after transfection, then total RNA and protein were extracted.

(A) The mRNA expression of CLDN5 is shown. The results are presented relative to pre-miR negative control transfected HUVEC. Mean ± SEM; ** p <0.01.

(B) CLDN5 protein expression in miR-125a transfected HUVEC. A representative figure from n = 4 individual experiments is shown, β-actin is applied as a loading control.

According to in silico prediction, there is no miR-125a binding site in the 3'UTR of CLDN5. The in silico target analysis is based on the prediction of canonical binding sites, that is, the 3'UTR of the mRNA contains the exact sequence of complementary bases in the miRNA seed region. In addition to canonical interactions, miRNA-mRNA regulation via non-canonical binding sites is also possible but has not yet been recognized by prediction algorithms. Luciferase reporter gene assays were performed to experimentally validate both canonical and non-canonical binding sites. For this purpose, the 3'UTR sequence of CLDN5 was cloned into the psiCHECK™-2 vector. Relative luciferase activity was determined and revealed no significant regulation of CLDN5 by miR-125a (Fig. 14).

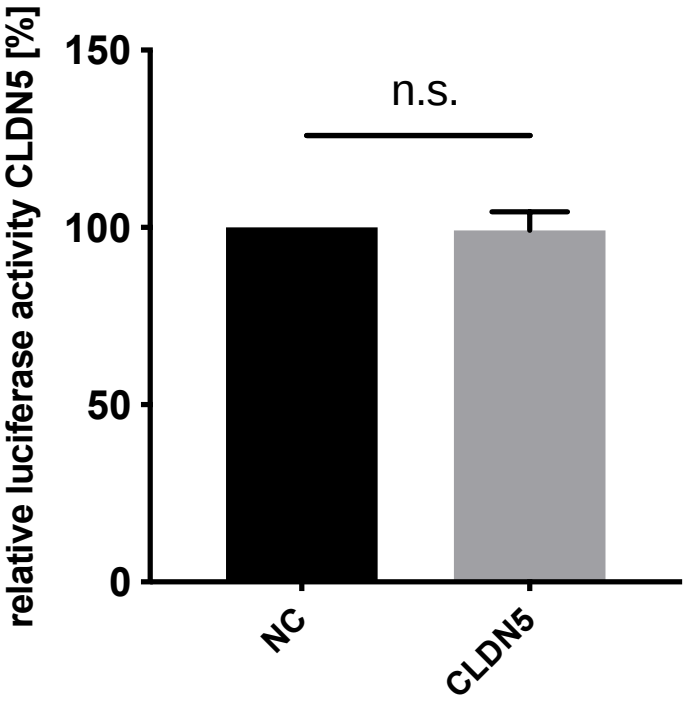

Figure 14 Indirect regulation of CLDN5 expression by miR-125a

Relative luciferase activity after co-transfection of pre-miR-125a or pre-miR negative control (NC) and the cloned CLDN5 psiCHECK™-2 dual luciferase vector. All experiments were carried out in triplicates. The values correspond to

Renilla-luciferase / Firefly-luciferase expression relative to the pre-miR negative control transfected HEK-293. Mean ± SEM; n.s. = not significant.

Recent evidence indicates that endothelial CDH5 mediates the expression of CLDN5[61], the question arose whether the expression of CDH5 and CLDN5 correlates with each other. Knock-down of either CDH5 or CLDN5 was performed by transfection of respective siRNA. Transfection of siCDH5 caused significant repression of CLDN5 on both mRNA (Fig. 15A) and protein (Fig. 15B) levels.

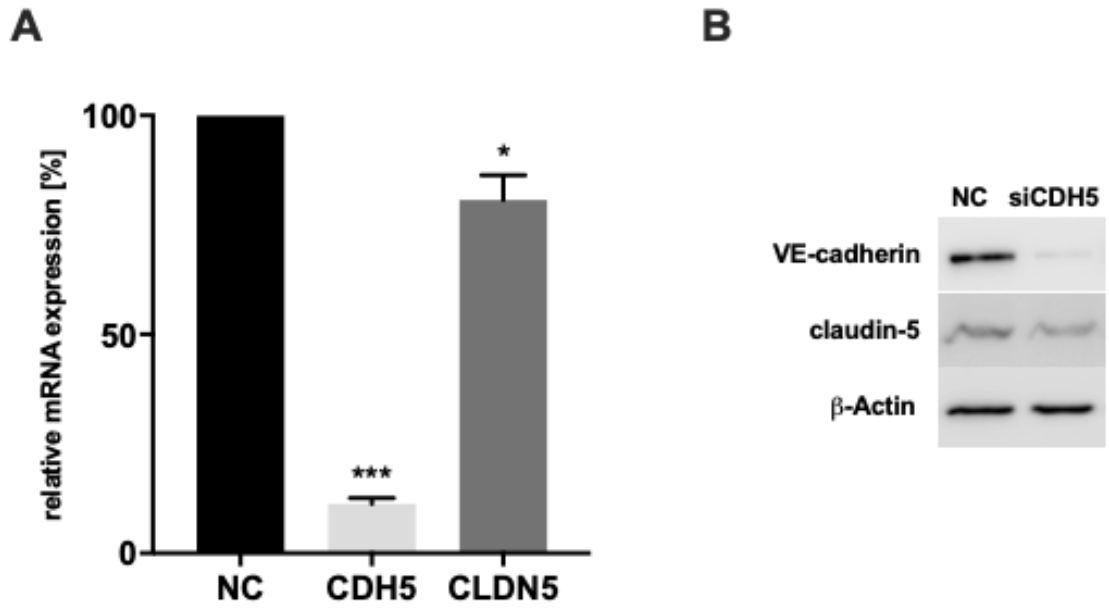

Figure 15 Knock-down of CDH5 reduces CLDN5 mRNA and protein expression

HUVEC were transfected with siCDH5 or Non-targeting siRNA (siNC) and stimulated with 25 ng/mL TNF for 24 hours.

(A) mRNA expression of CDH5 and CLDN5 were determined by qRT-PCR. CDH5 mRNA level is reduced by 88.7% ± 1.3%, n = 6, $p < 0.001$. CLDN5 mRNA level is reduced by 19.3% ± 5.7%, n = 6, $p < 0.05$. Mean ± SEM; * $p < 0.05$; *** $p < 0.001$.

(B) Total protein was extracted, and Western blot analysis was performed. A representative figure from n = 3 individual experiments is shown. CDH5 protein expression is repressed by 93.3% ± 1.5%, n = 3. CLDN5 protein level is decreased by 30.1% ± 7.3%, n = 3.

Furthermore, the knock-down of CLDN5 could in turn reduce the level of CDH5 in endothelial cells. After transfection of siCLDN5, the expression of endothelial CDH5 was significantly reduced (Fig. 16A). These results suggested a reciprocal expression inhibition of CDH5 and CLDN5, and CLDN5 appeared to be an indirect target of miR-125a.

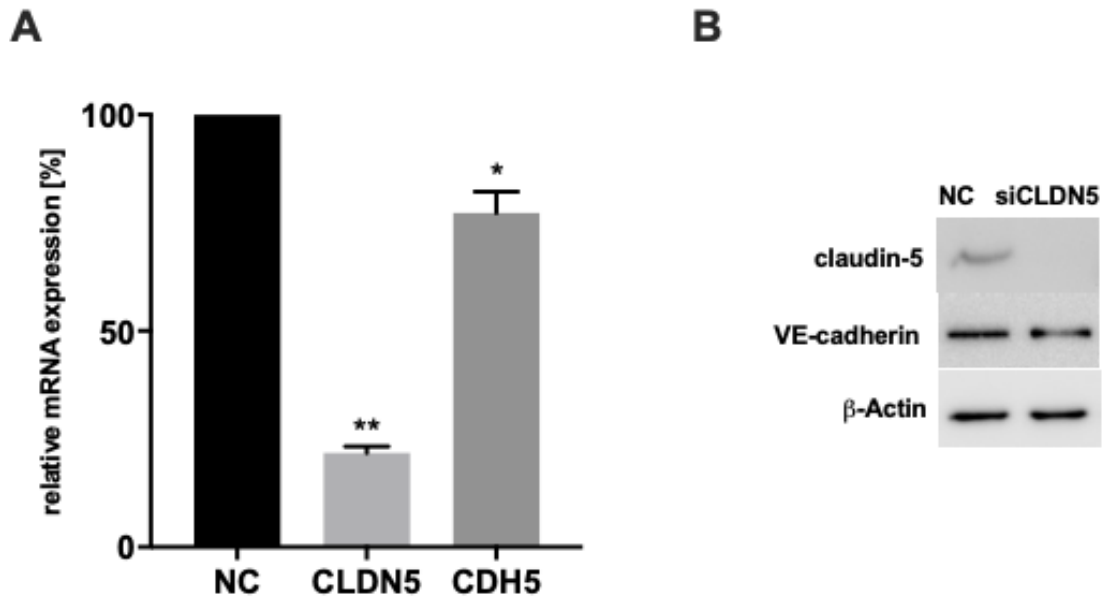

Figure 16 Knock-down of CLDN5 reduces CDH5 mRNA and protein expression

CLDN5 and CDH5 mRNA and protein expression after knock-down of CLDN5. HUVEC were harvested 48 hours after transfection and 6 hours 25 ng/mL TNF stimulation.

(A) CDH5 and CLDN5 mRNA expression was validated by qRT-PCR. CLDN5 mRNA level is reduced by 78.2% ± 1.5%, n = 5, $p < 0.01$. CDH5 mRNA level

is reduced by 22.8% ± 4.9%, n = 5, $p < 0.05$. Mean ± SEM; * $p < 0.05$; ** $p < 0.01$.

(B) Western blot analysis was performed after protein extraction. A representative figure from n = 3 individual experiments is shown. CLDN5 protein expression is repressed by 91.7% ± 1.1%, n = 3. CDH5 protein level is decreased by 25.6% ± 5.2%, n = 3.

3.6 The targets of miR-125a contribute to the endothelial hyperpermeable phenotype

In order to investigate whether PTPN1, PPP1CA, ETS1, and CLDN5 indeed explain the hyperpermeable phenotypes observed in miR-125a overexpressing endothelial cells. These targets were knocked down individually by transient transfection of the corresponding siRNA and the endothelial barrier function was tested. After gene-specific siRNA transfection, the knock-down efficiency of an individual target was evaluated by qRT-PCR (Fig. 17A-D).

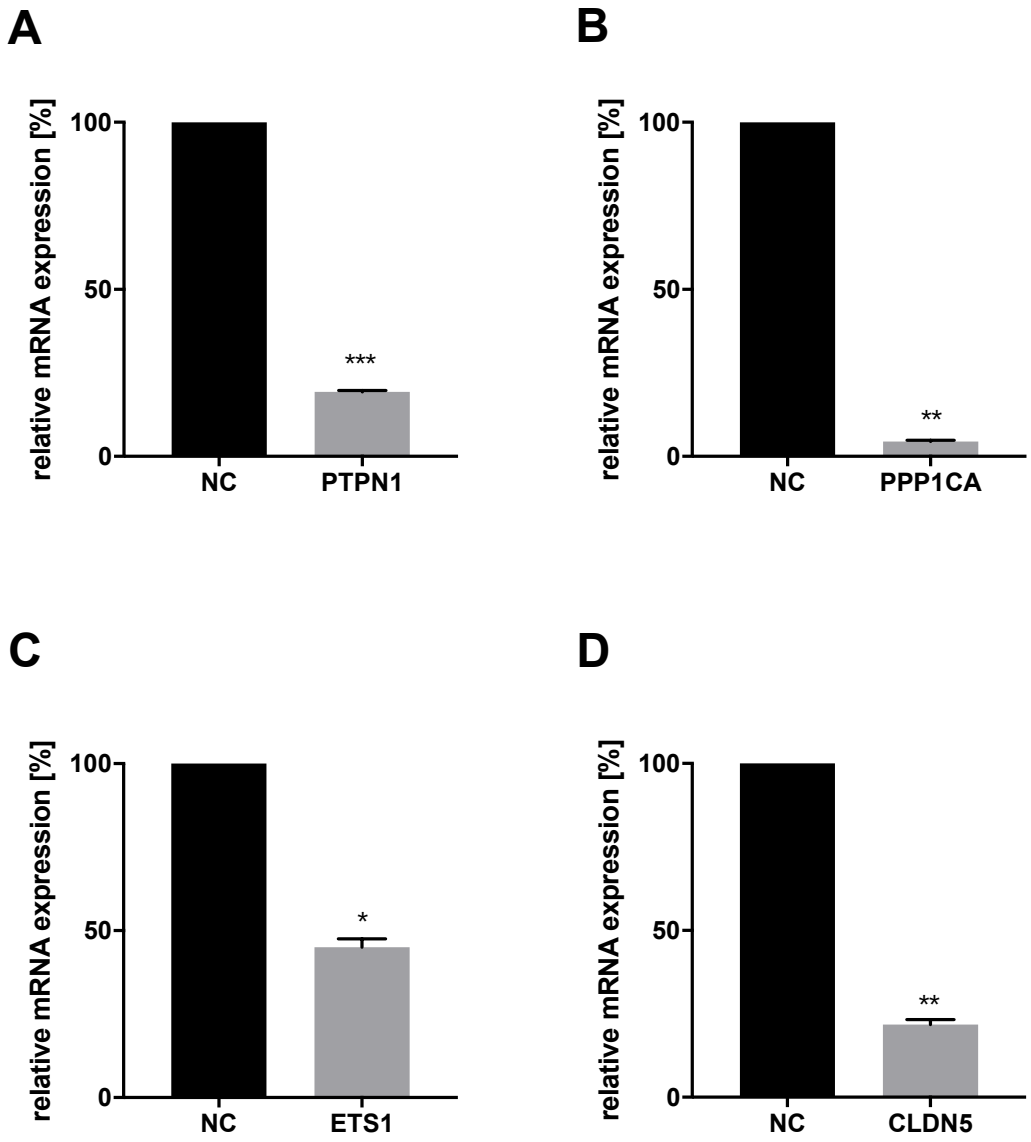

Figure 17　PTPN1, PPP1CA, ETS1, and CLDN5 mRNA levels after knock-down with respective siRNA

Total RNA was isolated 48 hours after HUVEC were transfected with respective siRNA or Non-targeting siRNA (siNC) and stimulated with 25 ng/mL TNF for 6 hours. Relative mRNA level of each target was determined by qRT-PCR.

(A) PTPN1 mRNA level is reduced by 80.7% ± 0.4%, n = 3, $p < 0.001$. Mean ± SEM; *** $p < 0.001$.

(B) PPP1CA mRNA level is reduced by 95.5% ± 0.3%, n = 3, $p < 0.01$. Mean ± SEM; ** $p < 0.01$.

(C) ETS1 mRNA level is reduced by 54.9% ± 2.5%, n = 3, $p < 0.05$. Mean ± SEM; * $p < 0.05$.

(D) CLDN5 mRNA level is reduced by 79.6% ± 1.9%, n = 3, $p < 0.01$. Mean ± SEM; ** $p < 0.01$.

As the indicator of cell barrier function, endothelial permeability and electric impedance were measured by permeability assays and ECIS® system, respectively. Knocking out CLDN5 enhanced TNF-induced increase in permeability (Fig. 18A). The real-time ECIS® results also indicated that the endothelial barrier function was impaired as the impedance of CLDN5 knockdown HUVEC monolayer was lower in basal conditions, and the impedance was extremely reduced when stimulated with TNF, area under the curve (AUC) was calculated for quantitatively evaluation (CLDN5: -17.1% ± 4.5%, n = 4, $p < 0.01$; Fig. 18B, C).

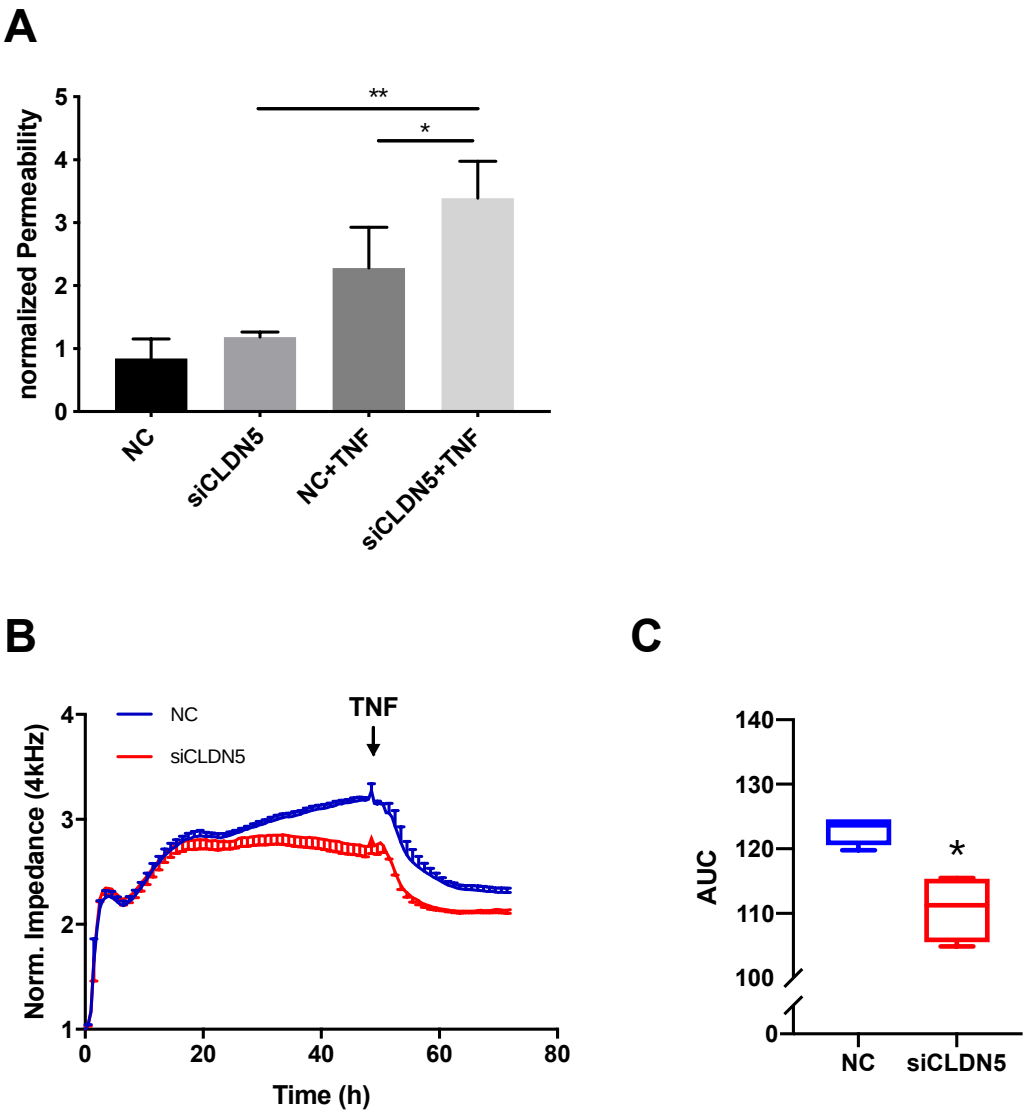

Figure 18　Knock-down of CLDN5 weakens endothelial barrier function

HUVEC were transfected with siCLDN5 or Non-targeting siRNA (siNC) and inoculated in cell culture inserts or ECIS® 8W10E+ PET arrays for 48 hours, and then stimulated with 25 ng/mL TNF stimulation for 24 hours. Permeability of HUVEC monolayer is represented by relative fluorescence intensity of medium collected from the lower compartments. The impedance was recorded at 4,000 Hz and normalized to the reference impedance measured before cell inoculation.

(A) With TNF stimulation, knock-down of CLDN5 increased HUVEC monolayer

permeability by 61.4% ± 16.2% (n = 4, $p < 0.05$). Mean ± SEM; * $p < 0.05$; ** $p < 0.01$.

(B) Decreased endothelial electrical impedance was observed in HUVEC transfected with siCLDN5 compared to siNC under basal and stimulated conditions.

(C) Area under the curve (AUC) was calculated from (E) for quantitative analysis. Mean ± SEM; n = 4; * $p < 0.05$.

Knock-down of PPP1CA or ETS1 did not affect endothelial barrier integrity under basal conditions but exacerbated endothelial barrier dysfunction upon TNF stimulation, as revealed by permeability assays (Fig. 19A, B) and ECIS® measurement (Fig. 19C-F). It indicated that the knockout of PPP1CA or ETS1 did not affect the formation of the endothelial barrier but aggravated barrier breakdown upon inflammatory stimulation.

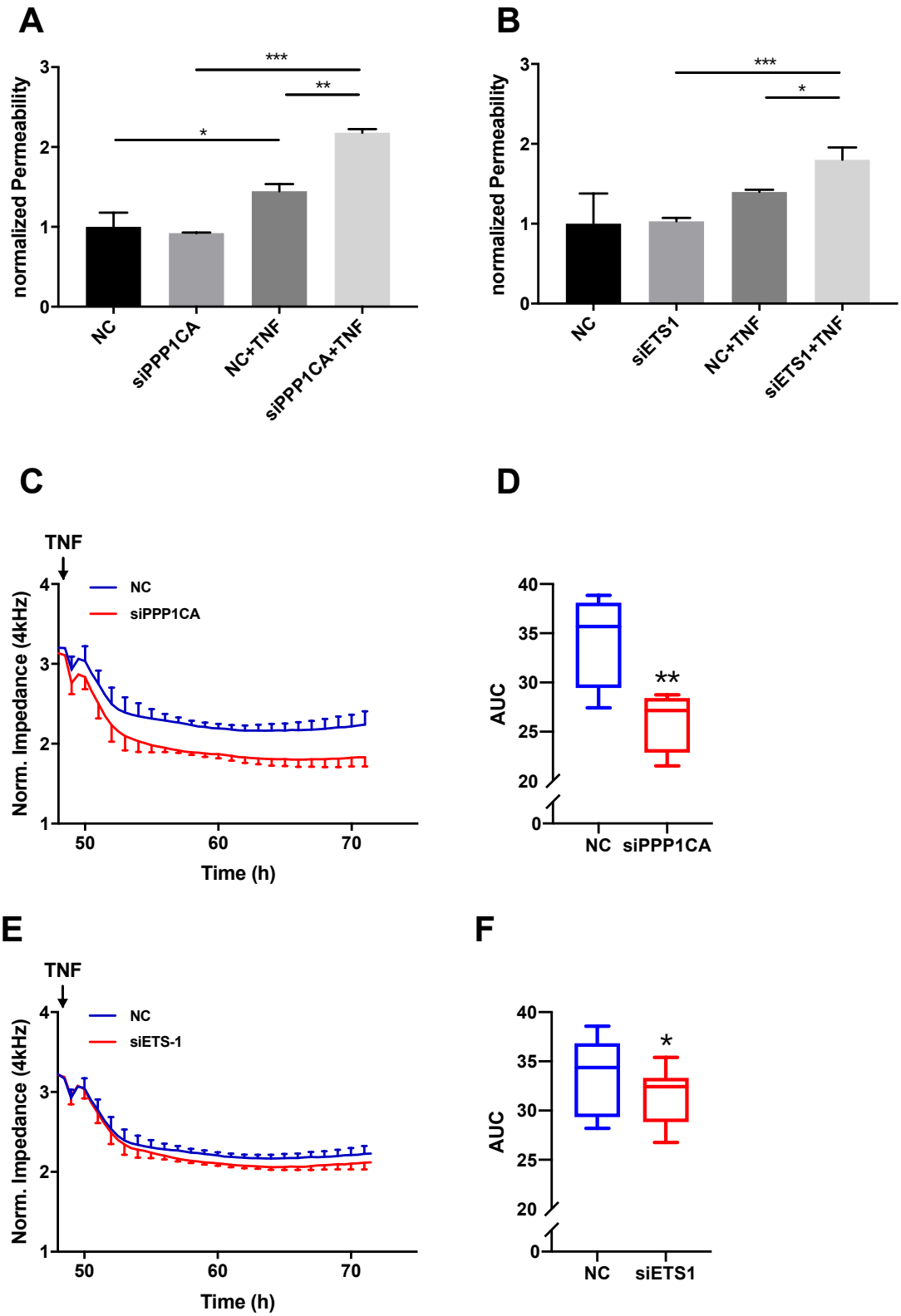
A
normalized Permeability
NC
siPPP1CA
NC+TNF
siPPP1CA+TNF
B
normalized Permeability
NC
siETS1
NC+TNF
siETS1+TNF
C
TNF
NC
siPPP1CA
Norm. Impedance (4kHz)
Time (h)
D
AUC
NC
siPPP1CA
E
TNF
NC
siETS-1
Norm. Impedance (4kHz)
Time (h)
F
AUC
NC
siETS1

Figure 19 Knock-down of PPP1CA or ETS1 exacerbates barrier destruction caused by TNF stimulation

Knock-down of PPP1CA or ETS1 in HUVEC was performed by transfection of respective siRNA. Transfected cells were inoculated in cell culture inserts or ECIS® 8W10E+ PET arrays for 48 hours followed by 24 hours of 25 ng/mL TNF stimulation. Permeability of HUVEC monolayer is represented by relative fluorescence intensity of medium collected from the lower compartments. Impedance was recorded over time at 4,000 Hz and normalized to the reference impedance measured before cell inoculation.

(A) Permeability of siPPP1CA transfected HUVEC increased by 52.1% ± 7.4% (n = 4, $p < 0.01$) upon TNF stimulation. Mean ± SEM; * $p < 0.05$; ** $p < 0.01$; *** $p < 0.001$.

(B) Knock-down of ETS1 increased HUVEC monolayer permeability by 36.9% ± 10.7% (n = 5, $p < 0.05$) upon TNF stimulation. Mean ± SEM; * $p < 0.05$; *** $p < 0.001$.

(C) After TNF stimulation, a greater decline of endothelial electrical impedance was observed in HUVEC transfected with siPPP1CA compared to siNC.

(D) Area under the curve (AUC) in siPPP1CA transfected HUVECS decreased by 23.8% ± 2.1% (n = 4, $p < 0.01$). Mean ± SEM; ** $p < 0.01$.

(E) ETS1 knock-down aggravated endothelial barrier breakdown shown by the reduction of endothelial electrical impedance under TNF stimulated conditions.

(F) Area under the curve (AUC) in siETS1 transfected HUVECS decreased by 5.0% ± 3.2% (n = 6, $p < 0.05$). Mean ± SEM; * $p < 0.05$.

There was no significant increase of macromolecule flux in permeability assays of PTPN1 knockdown endothelial monolayer (Fig. 20A). ECIS® measurement recorded that the impedance of HUVEC after PTPN1 knock-down decreased slightly (Fig. 20B, C). Western blot analysis revealed that upon TNF stimulation, PTPN1 knockdown resulted in a short-term increase of phosphorylated CDH5 (Fig. 20D). The transient internalization and degradation of CDH5 may explain the impedance variation detected in the real-time ECIS® system. In permeability assays, the endothelial barrier function was evaluated only 24 hours after TNF stimulation, and knockdown of PTPN1 was not sufficient to produce a sustainable effect.

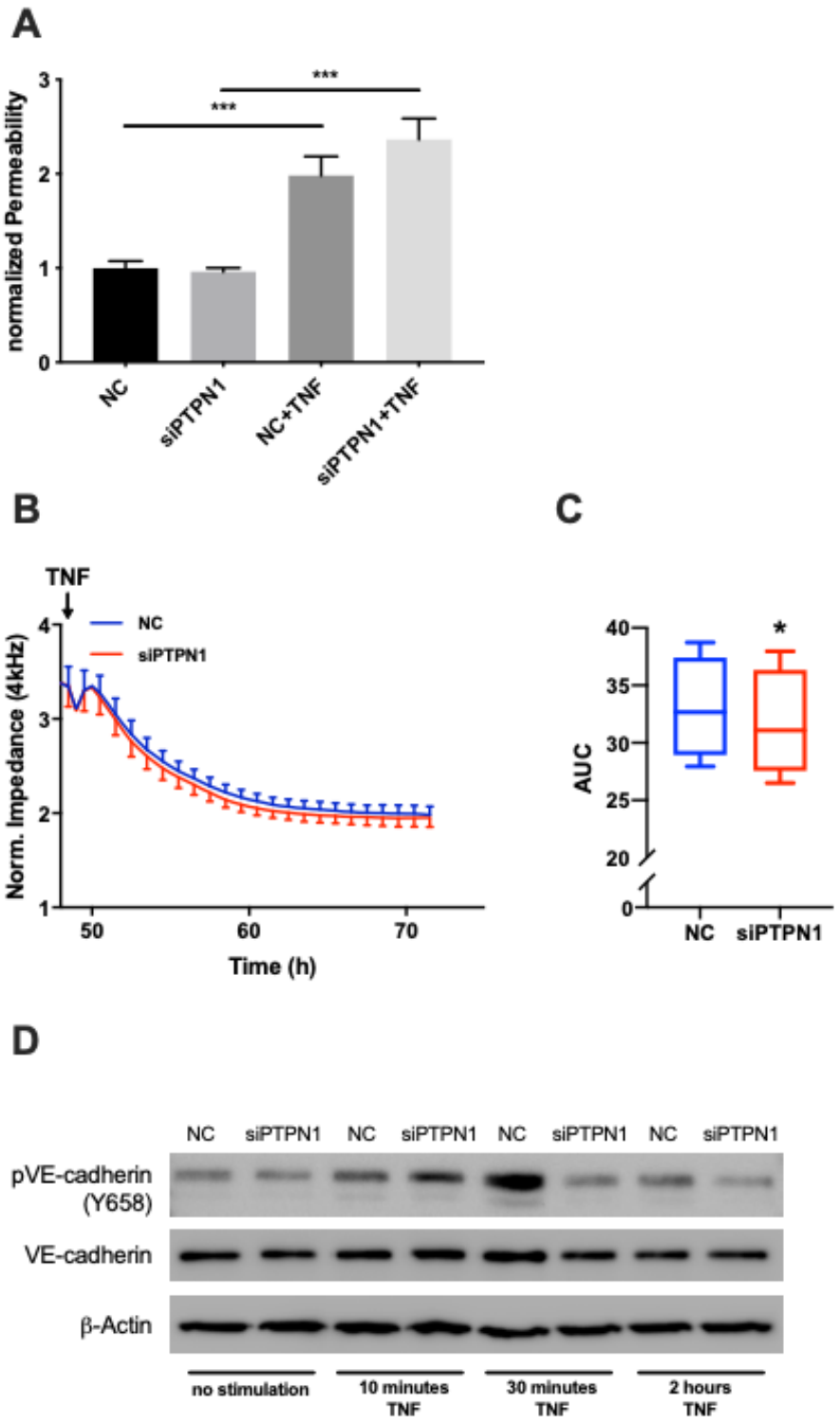

Figure 20 PTPN1 knock-down impairs endothelial barrier function by transiently increasing CDH5 phosphorylation

(A) In permeability assays, HUVEC were transfected with siPTPN1 or Non-

targeting siRNA (siNC) and incubated in cell culture inserts for 48 hours, then stimulated with 25 ng/mL TNF for 24 hours. There was no significant increase of relative fluorescence intensity in the PTPN1 knockdown HUVEC medium collected from the lower compartments.

(B) Impedance was recorded at 4,000 Hz. After TNF stimulation, compared with siNC, a slightly larger impedance drop was observed in HUVEC transfected with siPTPN1.

(C) Area under the curve (AUC) in siPTPN1 transfected HUVECS decreased by 4.2% ± 1.7% (n = 4, $p < 0.05$). Mean ± SEM; * $p < 0.05$.

(D) Protein expression of phosphorylated CDH5 (pVE-cadherin Y658) after knock-down of PTPN1. HUVEC were stimulated with 25 ng/mL TNF for 10 minutes, 30 minutes or 2 hours. Western blot analysis was performed after protein extraction. After 10 minutes of TNF stimulation, phosphorylated CDH5 protein expression is induced by 9.6% ± 1.1% (n = 3).

3.7 Inhibition of miR-125a can partially rescue the hyperpermeable phenotype

We could show that miR-125a impairs the barrier function of human endothelial cells by targeting PTPN1, PPP1CA, ETS1, and CLDN5 after inflammatory stimulation. Next, the effects of miR-125a inhibition were assessed. HUVEC were transfected with hsa-miR-125 miRNA inhibitor which reduced miR-125a level (Fig. 21).

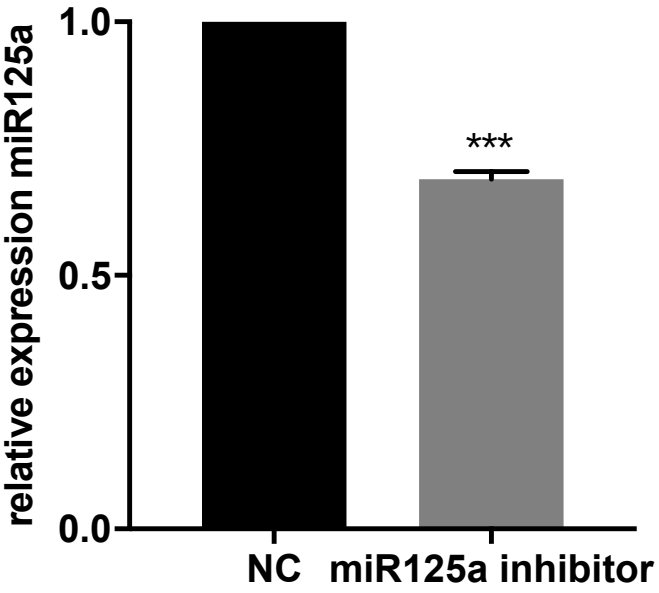

Figure 21 miR-125a level decreases in HUVEC after hsa-miR-125 miRNA inhibitor transfection

HUVEC were transfected with hsa-miR-125 miRNA inhibitor or Anti-miR™ Negative Control. Total RNA was isolated and TaqMan® MicroRNA Assay was used to quantify miR-125a expression. Relative endothelial miR-125a level decreased by 31.1% ± 1.5% (n = 4, $p < 0.001$) in HUVEC after hsa-miR-125 miRNA inhibitor transfection. Mean ± SEM; *** $p < 0.001$.

Inhibition of miR-125a also showed a clear induction of the mRNA expression of the four functional network targets: PTPN1: + 7.5% ± 2.5% (n = 11, $p < 0.05$); PPP1CA: + 8.4% ± 1.9% (n = 11, $p < 0.01$); ETS1: + 16.8% ± 5.0% (n = 7, $p < 0.01$); CLDN5: + 16.5% ± 4.4% (n = 10, $p < 0.05$; Fig. 22).

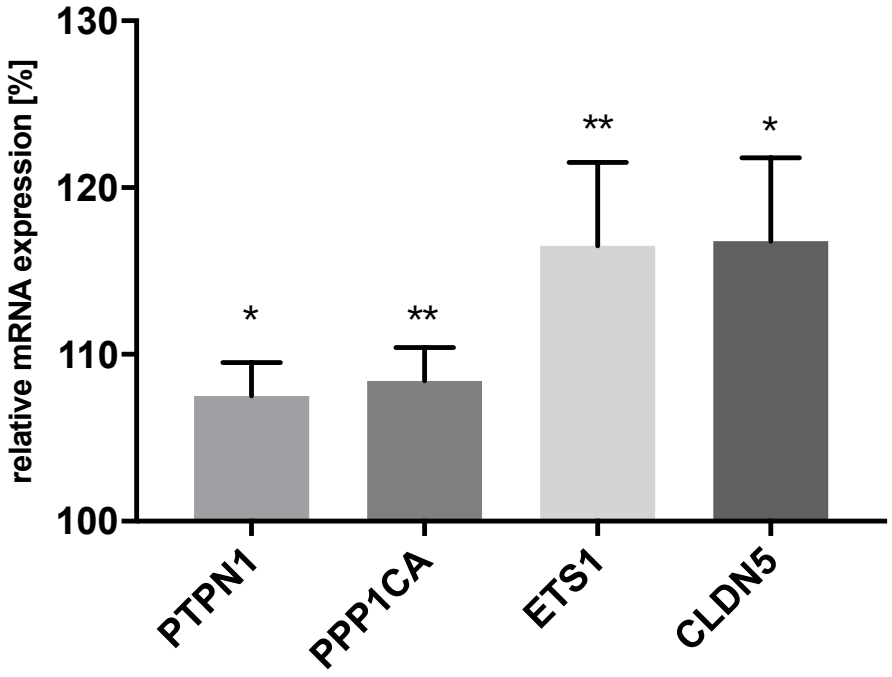

Figure 22 Inhibition of miR-125a increases mRNA levels of PTPN1, PPP1CA, ETS-1, and CLDN5 in endothelial cells

HUVEC were transfected with hsa-miR-125 miRNA inhibitor or Anti-miR™ Negative Control and stimulated with 25 ng/mL TNF for 6 hours. Relative mRNA levels of PTPN1, PPP1CA, ETS-1, and CLDN5 were determined by qRT-PCR. Mean ± SEM; * $p < 0.05$; ** $p < 0.01$.

Endothelial barrier function was assessed in miR-125a inhibitor transfected HUVEC. Permeability assays showed a reduction of TNF-induced FITC-albumin flux across hsa-miR-125 miRNA inhibitor transfected cell monolayer (- 10.42% ± 15.14%, n = 11, $p < 0.05$; Fig. 23A). Similarly, increased HUVEC monolayer impedance was observed in the ECIS® system (AUC + 2.3% ± 0.9%, n = 11, $p < 0.05$; Fig 23B, C). The results suggested that miR-125 inhibitor limited TNF-induced barrier dysfunction.

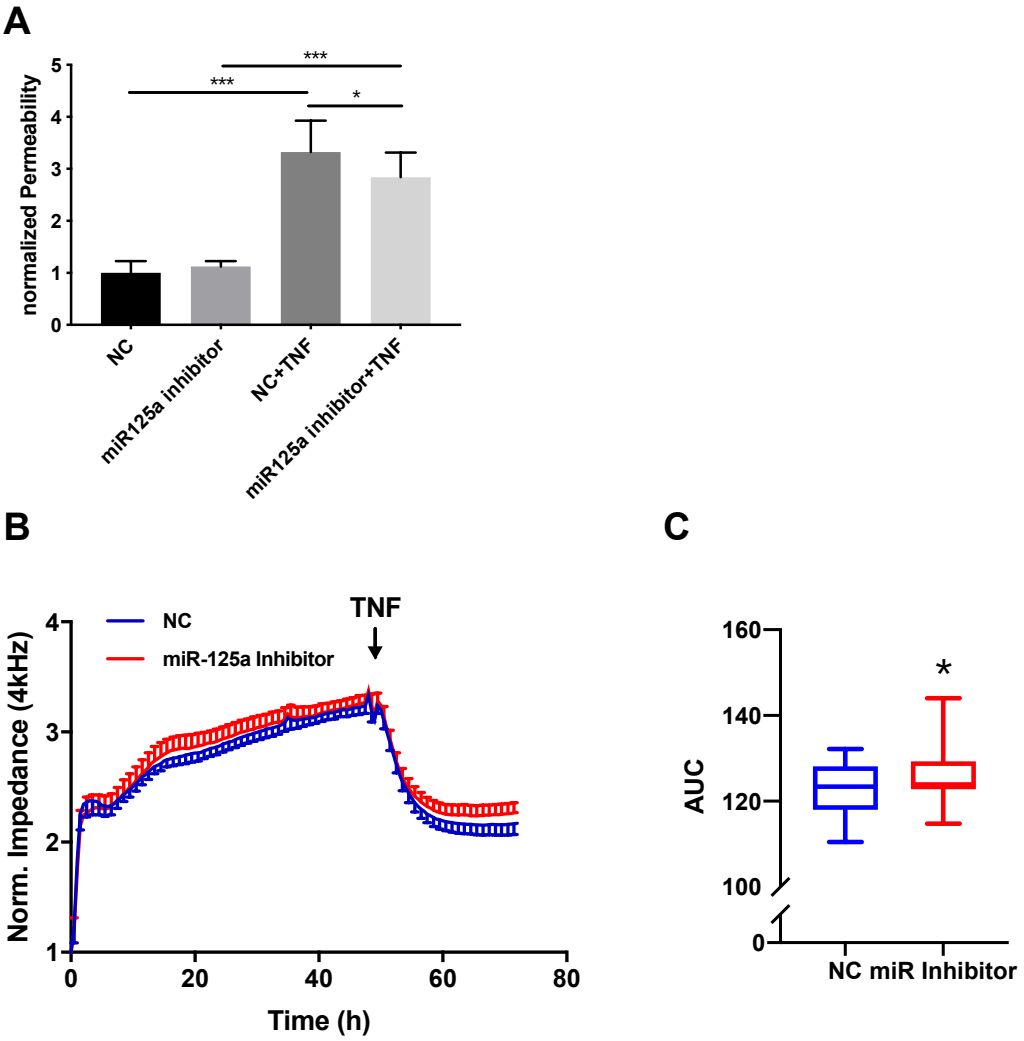

Figure 23 Inhibition of miR-125a can partially reverse the inflammation-induced high permeability phenotype of endothelial cells

(A) In permeability assays, transfection with miR-125 inhibitor decreased trans-endothelial passage of FITC-albumin after 24 h of TNF stimulation.

(B) Down-regulation of miR-125a expression by miR-125a inhibitor enhanced endothelial barrier function shown by increased endothelial electrical impedance.

(C) Area under the curve (AUC) in the miR-125 inhibitor transfected HUVECS increased by 2.3% ± 0.9% (n = 11, $p < 0.05$). Mean ± SEM; * $p < 0.05$.

4 Discussion

In the intact vasculature, the endothelium forms a continuous selective barrier that tightly controls the exchange between the circulation and surrounding tissues. Dysfunction of this barrier leads to uncontrolled fluid extravasation and tissue edema, which characterizes life-threatening conditions such as sepsis and acute lung injury[96]. In the process of acute inflammation, after stimulation by various pro-inflammatory mediators, different signaling pathways are induced in endothelial cells, leading to gap formation and barrier destruction[97]. In this study, we first identified that inflammation-induced miR-125a regulates endothelial barrier function under acute inflammatory conditions through a functional network consisting of the four targets PTPN1, PPP1CA, ETS-1, and CLDN5. Inhibition of miR-125a in endothelial cells can rescue this hyperpermeable phenotype.

In acute inflammation, pathogens could directly infect endothelial cells[98], but more commonly, endothelial cells are activated by a variety of host-derived factors, including cytokines, complement, chemokines[99], and changes in oxygenation or in blood flow[100, 101]. Impaired circulatory function is observed in systemic inflammation, leading to insufficient tissue perfusion and oxygenation. Here, we showed that intracellular miR-125a level was induced in endothelial cells in response to inflammatory stimuli and hypoxia.

Additionally, the level of miR-125a increased in extracellular vesicles isolated from the supernatants of stimulated HUVEC. Similarly, a recent study found that miR-125a expression in the serum of patients with sepsis was increased and is correlated with disease risk, severity, and prognosis[87]. Here, we provided evidence that the endothelial cells could be the source of this increased circulating miR-125a. Extracellular miRNAs bear high potential as diagnostic biomarkers[102, 103],

moreover, extracellular vesicle-mediated transfer of miRNA has attracted attention due to its effects on recipient cells, such as regulating protein expression[90]. The miRNAs could be selectively packaged into extracellular vesicles and subsequently released into the circulatory system or the surrounding tissue[104]. In this way, miR-125a could be transported from the site of acute inflammation to the more distant vascular bed, thus exhibiting systemic hyperpermeable effects. However, there are still relatively few studies on mechanisms of circulating miRNA, especially with the ultimate goal of providing therapy.

Overexpression of miR-125a in endothelial cells weakened endothelial barrier function, which is manifested as an increase in the permeability of endothelial monolayer under basal and TNF-stimulated conditions. In addition to permeability assays, which measure endothelial barrier properties at fixed time points, the electrical impedance of the endothelial monolayer was measured by the ECIS® system in real-time. Impairment of the endothelial barrier function results in a decrease in impedance. Overexpression of miR-125a reduced the impedance of the endothelial monolayer, indicating an impaired endothelial barrier function. After cell inoculation, the electrical impedance values of the two groups of cells transfected with pre-miR-125a or the pre-miR negative control were basically the same, indicating that the two groups of cells evenly covered the bottom of the culture well. However, when the cell-to-cell junctions were established later, the difference had already appeared. The endothelial cells overexpressing miR-125a can only build a weaker barrier, which was manifested by a lower electrical impedance value. After TNF stimulation, the barrier function was further destroyed, and the electrical impedance value dropped significantly to the state before the establishment of the junctions between cells. This indicates that overexpression of miR-125a impairs endothelial barrier formation and integrity.

Based on their regulatory mechanism, miRNAs act as transcriptional regulators in functional networks, where one miRNA may regulate many genes as its targets, while multiple miRNAs target the same gene. As an important component of vast regulatory networks, miRNAs enhance their regulatory potential by simultaneously targeting related signal cascades molecules[105, 106].

After miR-125a overexpression in endothelial cells, RNA sequencing was performed, and the results of the Next Generation Sequencing were evaluated by bioinformatics. A disproportionately high number of genes that are key components of the *GO_regulation of cell adhesion* and *KEGG_adherens junctions* pathway were identified as regulated by miR-125a. With the help of the in silico analysis and reporter gene assays, three direct targets (ETS-1, PTPN1, PPP1CA) were finally confirmed, which may explain the barrier hyperpermeability exhibited in endothelial cell overexpressing miR-125a. In addition to directly binding to target gene mRNA to inhibit its translation and protein synthesis, miR-125a can also affect the expression of other genes, such as CLDN5, through indirect regulation. The overexpression of miR-125a as well as independent knockdown of each individual network target increased permeability and decreased the impedance of the endothelial monolayer, confirming this network hypothesis.

The complex miR-125a functional network is composed of two adhesion molecules CDH5 and CLDN5. CDH5 and CLDN5 genes encode VE-cadherin and claudin-5, respectively. Being the major component of the vascular endothelial cell junction, VE-cadherins sustain intercellular adherens junctions and modulate endothelial permeability[26]. In endothelial cells, VE-cadherin is required for vascular development and remodeling in the embryo[107, 108]. In adults, the expression and organization of VE-cadherin at endothelial junctions are critical for vascular stability[109]. Tight junction adhesive protein claudin-5 is an indispensable membrane

protein, which determines the paracellular permeability of endothelial monolayer by regulating the flux of water-soluble molecules between adjacent cells[61]. In this study, endothelial cells with CLDN5 knock-down only formed a weak barrier, with later superimposed TNF stimulation exacerbated the barrier damage. As the major participants in endothelial barrier function, the expression of CDH5 and CLDN5 was inhibited by the overexpression of miR-125a induced by inflammatory stimuli, thereby affecting the establishment and integrity of the endothelial barrier.

Furthermore, the miR-125a network not only acts through direct miRNA-mRNA interaction but also through inter-target regulatory crosstalk that enhances its effect. Besides the two adhesion molecules mentioned above, there are two regulatory tyrosine phosphatases (PTPN1, PPP1CA) and one transcription factor (ETS-1) in this miR-125a network. The mutual regulation of these miR-125a target genes also contributes to this regulatory network.

In in silico analysis, the miR-125a binding site was not found in the 3'UTR of CLDN5. In order to verify whether miR-125a regulates CLDN5 mRNA via non-canonical binding sites, luciferase reporter gene assays were performed and revealed no significant regulation of CLDN5 by miR-125a. However, recent studies found that the clustering of VE-cadherin on the cell membrane induces the expression of claudin-5 by inhibiting the effects of FoxO1 and nuclear translocation of β-catenin [61]. These results provide evidence that adherens junctions and tight junctions are positively interconnected. In this study, we found a reciprocal regulation of CDH5 and CLDN5 on mRNA and protein levels by knocking down each adhesion molecule. CLDN5 represents another component of the miR-125a functional network in the regulation of endothelial barrier function. In addition to controlling the adhesion properties of fluid exchange across endothelial cells, junction proteins can also transfer intracellular signals to regulate gene expression[110, 111]. Tight junctions and adherens junctions

are functionally linked, but the mechanism of this crosstalk still needs further exploration.

Different from the adhesion molecules CDH5 and CLDN5, the other three miR-125a network targets ETS1, PTPN1, and PPP1CA are not part of cell-to-cell junctions, but indirectly participate in the regulation of endothelial barrier function by modulating endothelial activation. As expected, knock-down of ETS1, PTPN1, or PPP1CA causes endothelial barrier hyperpermeability only after TNF treatment, since they regulate endothelial response to inflammatory stimulation.

ETS-1 has recently been confirmed as a direct target of miR-125a[94, 112]. Upon inflammatory stimulation, such as TNF, endothelial cells compensate for the degradation of surface VE-cadherin by upregulating transcription factor ETS1 in an NF-κB dependent manner and promoting the de novo synthesis of VE-cadherin[48]. Thus, ETS1 affects paracellular permeability by regulating VE-cadherin expression in response to TNF. Consistent with our research, ETS-1 knockdown only caused barrier impairment in TNF-stimulated endothelial cells.

VE-cadherin phosphorylation status and unstable expression on the endothelial cell surface are the main triggers for endothelial activation in response to inflammation[50]. PTPN1 is a novel miR-125a target, which encodes protein phosphatase 1B (PTP1B). The protein phosphatase PTP1B reduces tyrosine phosphorylation of VE-cadherin by negatively regulating the activation of the VEGFR2 receptor, thereby stabilizing the adherens junctions and endothelial barrier in acute inflammation[113]. In our study, PTPN1 knock-down did not increase the permeability of endothelial cell monolayer and only had a slightly larger impedance drop after TNF stimulation. Inflammatory mediators could instantly activate the phosphorylation of VE-cadherin and cause the remodeling of adherens junctions[25]. Here, we profiled the time-dependent VE-

cadherin phosphorylation kinetics in PTPN1 knock-down HUVEC. An increase in phosphorylated VE-Cadherin was detected only ten minutes after TNF stimulation. The dephosphorylation of VE-cadherin by PTP1B upon inflammatory stimulation is a short-term effect. This result explains why it is difficult to detect changes in endothelial barrier function by permeability assay or ECIS.

PPP1CA has been confirmed as a direct target of miR-125a[95] and code for PP1α, which is one of the catalytic subunits of the protein phosphatase 1 (PP1). PP1 belongs to a serine/threonine phosphatase family and plays a role in multiple signaling pathways involved in angiogenic processes and endothelial permeability[114, 115]. The phosphatase dephosphorylates myosin regulatory light chain, restricts the interaction of myosin with actin filaments of the cytoskeleton, and subsequently stabilizes the VE-cadherin junction complex[116]. By activating the actin-myosin contractile machinery, inhibition of PP1 leads to endothelial barrier leakage upon inflammatory stimulation.

Our study underlines the complexity of the miRNA-related functional network. This field initially focused on identifying novel targets of individual miRNAs. In the last decade, the research of miRNAs ushers in a new era, that is, not limited to establishing individual connections between miRNAs and predicted targets, but also focusing on networks[117]. Our research further shows that although miR-125a is the center of the establishment of this endothelial barrier regulatory network, it is not limited to this. The target genes of miR-125a can also influence the expression and function of each other on different levels by transcriptional activation (CLDN5, ETS-1 and CDH5), inhibition of degradation (PTPN1), or via actin reorganization (PPP1CA). Thus, making this regulatory network more refined and have greater potential. The schematic diagram of the miR-125a functional network is summarized in Figure 24.

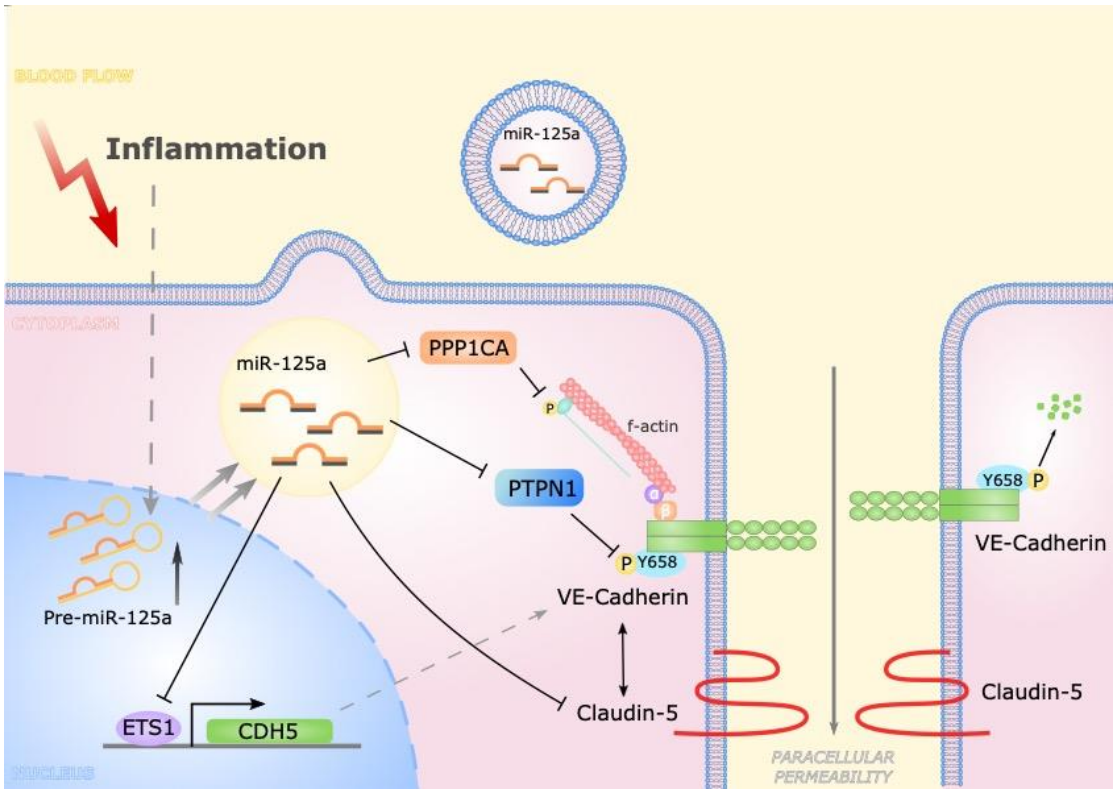

Figure 24 Schematic illustration of miR-125a network effects on endothelial barrier integrity during inflammation

In response to inflammatory stimulation, the expression of miR-125a increases in endothelial cells and is released through extracellular vesicles. MiR-125a directly regulates PTPN1, PPP1CA, and ETS-1, while the expression of the indirect target CLDN5 is reciprocally linked to CDH5 expression. In addition, by targeting PTPN1 and PPP1CA, miR-125a inhibits the dephosphorylation of VE-Cadherin and the myosin regulatory light chain, thus affecting the stabilization of adherens junctions and actin cytoskeleton. miR-125a constitutes second-order repression on CDH5 transcriptional activity by reducing the expression of ETS-1.

The characteristics of miRNA expressed in different tissues are highly specific and can shape the features and functions of tissues[118]. Specific miRNA expression patterns

have been identified for a variety of human diseases including cancer, cardiovascular diseases, and inflammatory diseases and miRNAs have been recognized as important clinical biomarkers for the diagnosis of specific diseases[66, 67, 119]. Due to their regulative capability, miRNAs are also considered as potential therapeutic targets. For diseases with a clear causal relationship between the altered miRNAs expression profile and the pathological states, both synthetic miRNA mimics and inhibitors have been developed and made their way into different clinical studies, representing a new field of modern medicine research[70]. For the strategy of upregulating miRNA expression levels, miRNA mimics interact with RNA-induced silencing complex (RISC) and target mRNA for early degradation[120]. For miRNA downregulation strategies, such as anti-miRNA oligonucleotides (AMOs)[121], miRNA molecular inhibitors of specific miRNA[122], or miRNA sponges[123], can target miRNA generation or prevent miRNA and mRNA interaction.

In our study, the specific miR-125a inhibitor upregulated PTPN1, PPP1CA, ETS1, and CLDN5 mRNA levels in HUVEC and ameliorated TNF-induced endothelial barrier dysfunction in vitro. This specific miRNA inhibitor may have the potential as a therapeutic method to restore the integrity of the endothelial barrier in acute inflammatory diseases such as sepsis or ARDS. However, the development of this area is still relatively slow compared to the development of therapeutic overexpression of miRNA strategies. Further investigations are needed to determine whether the small molecular miR-125a inhibitor benefits in the restoration of a disrupted endothelial barrier function in acute inflammatory conditions in vivo.

The destruction of endothelial barrier function is a fundamental pathophysiological event that occurs in the early stage of acute inflammatory conditions such as sepsis[16]. In the last decade, animal studies have shown that preventing vascular leakage can reduce the severity of sepsis complications and the mortality rate of sepsis[124-126],

and great efforts have been made in numerous clinical trials focused on restoring the impaired endothelial barrier under acute inflammatory conditions. However, so far, there is no clinically effective treatment method to restore endothelial barrier dysfunction under acute inflammatory conditions. The miR-125a functional network identified in our study helps to understand the complex molecular mechanisms of endothelial barrier dysfunction in acute inflammatory conditions, paving the way for potential new treatment strategies.

Summary

Increased endothelial permeability is a prominent feature of acute inflammatory diseases, where leakage can result in edema, impaired function, and morbidity. Hyperpermeability is characterized by the disruption of endothelial junctions. The exact molecular mechanisms of the downregulation of endothelial adhesion molecules, however, are currently not clear. MicroRNAs (miRNAs) post-transcriptionally regulate gene expression in a network pattern. Recent studies have revealed that the inflammatory inducible expression of miRNAs could play an important role in regulating endothelial barrier functions during inflammation. The miR-125 family has been reported to play a crucial role in a variety of cellular processes, including endothelial cell tube formation of blood vessels. Circulating miR-125a was found to be elevated in blood samples of patients with acute inflammation such as sepsis and correlated with disease severity. Therefore, we aimed to investigate the impact of miR-125a on the endothelial barrier function during acute inflammation and determine the functional network of miR-125a.

Human umbilical vein endothelial cells (HUVEC) were isolated from the umbilical cords by collagenase treatment. After inflammatory stimulation, the induction of MicroRNA was verified in HUVEC or cell supernatant. HUVEC were transfected with microRNA, specific target siRNAs, or miRNA inhibitors by electroporation. The transcriptome of HUVEC overexpressing miR-125a was analyzed using Next Generation Sequencing (NGS) followed by bioinformatics pathway analysis. Results were experimentally validated via real-time PCR, western blots, and immunofluorescence. Reporter gene assays were performed to validate direct targets of miR-125a. Endothelial barrier function was measured by permeability assay and Electric Cell-substrate Impedance Sensing (ECIS®).

Upregulation of miR-125a level was observed in HUVEC and extracellular vesicles after inflammatory stimulation. The results of the NGS were evaluated bioinformatically and showed that after miR-125a overexpression, a large number of genes that are key components of the cell adhesion pathway were disproportionately and significantly regulated. Overexpression of miR-125a in HUVEC resulted in a significant increase in permeability of the endothelial cell monolayer and a decrease in barrier impedance. Reporter gene assays identified PTPN1 as previously unknown direct targets of miR-125a. CLDN5 expression was reciprocally regulated by CDH5 expression and represented an indirect target of miR-125a. PPP1CA and ETS-1 are already published targets of miR-125a. The specific knockdown of each of the three targets impaired endothelial barrier function, thus confirming a specific functional network of miR-125a. On the contrary, inhibition of miR-125a can partially rescue the hyperpermeable phenotype caused by inflammatory stimuli.

Taken together, miR-125a expression is induced in endothelial cells upon inflammatory stimulation and regulates endothelial barrier dysfunction by simultaneous targeting of PTPN1, PPP1CA, ETS1, and CLDN5. This newly identified miR-125a functional network could be a novel molecular mechanism involved in endothelial barrier dysfunction during acute inflammation.

References

1. Kruger-Genge, A., et al., *Vascular Endothelial Cell Biology: An Update.* Int J Mol Sci, 2019. **20**(18).
2. Shao, Y., et al., *Vascular Endothelial Cells and Innate Immunity.* Arterioscler Thromb Vasc Biol, 2020. **40**(6): p. e138-e152.
3. Ince, C., et al., *The Endothelium in Sepsis.* Shock, 2016. **45**(3): p. 259-70.
4. Zhong, L., M.J. Simard, and J. Huot, *Endothelial microRNAs regulating the NF-kappaB pathway and cell adhesion molecules during inflammation.* FASEB J, 2018. **32**(8): p. 4070-4084.
5. Muller, W.A. and G.J. Randolph, *Migration of leukocytes across endothelium and beyond: molecules involved in the transmigration and fate of monocytes.* J Leukoc Biol, 1999. **66**(5): p. 698-704.
6. Leng, B., et al., *Astragaloside IV improves vascular endothelial dysfunction by inhibiting the TLR4/NF-kappaB signaling pathway.* Life Sci, 2018. **209**: p. 111-121.
7. Wang, W., et al., *TLR4 activation induces nontolerant inflammatory response in endothelial cells.* Inflammation, 2011. **34**(6): p. 509-18.
8. Studt, J.D., et al., *Fatal congenital thrombotic thrombocytopenic purpura with apparent ADAMTS13 inhibitor: in vitro inhibition of ADAMTS13 activity by hemoglobin.* Blood, 2005. **105**(2): p. 542-4.
9. Nolasco, L.H., et al., *Hemolytic uremic syndrome-associated Shiga toxins promote endothelial-cell secretion and impair ADAMTS13 cleavage of unusually large von Willebrand factor multimers.* Blood, 2005. **106**(13): p. 4199-209.
10. Levi, M. and T. van der Poll, *Coagulation and sepsis.* Thromb Res, 2017. **149**: p. 38-44.
11. Radeva, M.Y. and J. Waschke, *Mind the gap: mechanisms regulating the endothelial barrier.* Acta Physiol (Oxf), 2018. **222**(1).
12. Sarelius, I.H. and A.J. Glading, *Control of vascular permeability by adhesion molecules.* Tissue Barriers, 2015. **3**(1-2): p. e985954.
13. Aird, W.C., *The role of the endothelium in severe sepsis and multiple organ dysfunction syndrome.* Blood, 2003. **101**(10): p. 3765-77.

14. Wettschureck, N., B. Strilic, and S. Offermanns, *Passing the Vascular Barrier: Endothelial Signaling Processes Controlling Extravasation.* Physiol Rev, 2019. **99**(3): p. 1467-1525.

15. Alsaffar, H., et al., *Interleukin-6 promotes a sustained loss of endothelial barrier function via Janus kinase-mediated STAT3 phosphorylation and de novo protein synthesis.* Am J Physiol Cell Physiol, 2018. **314**(5): p. C589-C602.

16. Dolmatova, E.V., et al., *The effects of sepsis on endothelium and clinical implications.* Cardiovasc Res, 2021. **117**(1): p. 60-73.

17. Batah, S.S. and A.T. Fabro, *Pulmonary pathology of ARDS in COVID-19: A pathological review for clinicians.* Respir Med, 2021. **176**: p. 106239.

18. Cecconi, M., et al., *Sepsis and septic shock.* Lancet, 2018. **392**(10141): p. 75-87.

19. MD, H. and D. AM, - *Management of Sepsis and Septic Shock.* - JAMA. 2017 Feb 28;317(8):847-848. doi: 10.1001/jama.2017.0131., (- 1538-3598 (Electronic)): p. - 847-848.

20. Deutschman, C.S. and K.J. Tracey, *Sepsis: current dogma and new perspectives.* Immunity, 2014. **40**(4): p. 463-75.

21. Komarova, Y.A., et al., *Protein Interactions at Endothelial Junctions and Signaling Mechanisms Regulating Endothelial Permeability.* Circ Res, 2017. **120**(1): p. 179-206.

22. Frye, M., et al., *Interfering with VE-PTP stabilizes endothelial junctions in vivo via Tie-2 in the absence of VE-cadherin.* J Exp Med, 2015. **212**(13): p. 2267-87.

23. Tietz, S. and B. Engelhardt, *Brain barriers: Crosstalk between complex tight junctions and adherens junctions.* J Cell Biol, 2015. **209**(4): p. 493-506.

24. Duong, C.N. and D. Vestweber, *Mechanisms Ensuring Endothelial Junction Integrity Beyond VE-Cadherin.* Front Physiol, 2020. **11**: p. 519.

25. Vestweber, D., et al., *Cell adhesion dynamics at endothelial junctions: VE-cadherin as a major player.* Trends Cell Biol, 2009. **19**(1): p. 8-15.

26. Giannotta, M., M. Trani, and E. Dejana, *VE-cadherin and endothelial adherens junctions: active guardians of vascular integrity.* Dev Cell, 2013. **26**(5): p. 441-54.

27. Vestweber, D., *VE-cadherin: the major endothelial adhesion molecule controlling cellular junctions and blood vessel formation.* Arterioscler Thromb Vasc Biol, 2008. **28**(2): p. 223-32.

28. Dejana, E. and C. Giampietro, *Vascular endothelial-cadherin and vascular stability.* Curr Opin Hematol, 2012. **19**(3): p. 218-23.

29. Morini, M.F., et al., *VE-Cadherin-Mediated Epigenetic Regulation of Endothelial Gene Expression.* Circ Res, 2018. **122**(2): p. 231-245.

30. Lampugnani, M.G., *Endothelial adherens junctions and the actin cytoskeleton: an 'infinity net'?* J Biol, 2010. **9**(3): p. 16.

31. Grimsley-Myers, C.M., et al., *VE-cadherin endocytosis controls vascular integrity and patterning during development.* J Cell Biol, 2020. **219**(5).

32. Hagerling, R., et al., *Distinct roles of VE-cadherin for development and maintenance of specific lymph vessel beds.* EMBO J, 2018. **37**(22).

33. Cong, X. and W. Kong, *Endothelial tight junctions and their regulatory signaling pathways in vascular homeostasis and disease.* Cell Signal, 2020. **66**: p. 109485.

34. Kakogiannos, N., et al., *JAM-A Acts via C/EBP-alpha to Promote Claudin-5 Expression and Enhance Endothelial Barrier Function.* Circ Res, 2020.

35. Greene, C., N. Hanley, and M. Campbell, *Claudin-5: gatekeeper of neurological function.* Fluids Barriers CNS, 2019. **16**(1): p. 3.

36. Simske, J.S., *Claudins reign: The claudin/EMP/PMP22/gamma channel protein family in C. elegans.* Tissue Barriers, 2013. **1**(3): p. e25502.

37. Nitta, T., et al., *Size-selective loosening of the blood-brain barrier in claudin-5-deficient mice.* J Cell Biol, 2003. **161**(3): p. 653-60.

38. Greene, C., et al., *Dose-dependent expression of claudin-5 is a modifying factor in schizophrenia.* Mol Psychiatry, 2018. **23**(11): p. 2156-2166.

39. Morita, K., et al., *Endothelial claudin: claudin-5/TMVCF constitutes tight junction strands in endothelial cells.* J Cell Biol, 1999. **147**(1): p. 185-94.

40. Mandell, K.J. and C.A. Parkos, *The JAM family of proteins.* Adv Drug Deliv Rev, 2005. **57**(6): p. 857-67.

41. Kakogiannos, N., et al., *JAM-A Acts via C/EBP-alpha to Promote Claudin-5 Expression and Enhance Endothelial Barrier Function.* Circ Res, 2020. **127**(8): p. 1056-1073.

42. Duong, C.N., et al., *Interference With ESAM (Endothelial Cell-Selective Adhesion Molecule) Plus Vascular Endothelial-Cadherin Causes Immediate Lethality and Lung-Specific Blood Coagulation.* Arterioscler Thromb Vasc Biol, 2020. **40**(2): p. 378-393.

43. Pober, J.S. and W.C. Sessa, *Evolving functions of endothelial cells in inflammation.* Nat Rev Immunol, 2007. **7**(10): p. 803-15.

44. Gunduz, D., et al., *ATP antagonism of thrombin-induced endothelial barrier permeability.* Cardiovasc Res, 2003. **59**(2): p. 470-8.

45. Wojciak-Stothard, B. and A.J. Ridley, *Rho GTPases and the regulation of endothelial permeability.* Vascul Pharmacol, 2002. **39**(4-5): p. 187-99.

46. Aslam, M., et al., *cAMP/PKA antagonizes thrombin-induced inactivation of endothelial myosin light chain phosphatase: role of CPI-17.* Cardiovasc Res, 2010. **87**(2): p. 375-84.

47. Xiong, S., et al., *IL-1beta suppression of VE-cadherin transcription underlies sepsis-induced inflammatory lung injury.* J Clin Invest, 2020. **130**(7): p. 3684-3698.

48. Colas-Algora, N., et al., *Compensatory increase of VE-cadherin expression through ETS1 regulates endothelial barrier function in response to TNFalpha.* Cell Mol Life Sci, 2020. **77**(11): p. 2125-2140.

49. Adam, A.P., *Regulation of Endothelial Adherens Junctions by Tyrosine Phosphorylation.* Mediators Inflamm, 2015. **2015**: p. 272858.

50. Potter, M.D., S. Barbero, and D.A. Cheresh, *Tyrosine phosphorylation of VE-cadherin prevents binding of p120- and beta-catenin and maintains the cellular mesenchymal state.* J Biol Chem, 2005. **280**(36): p. 31906-12.

51. Orsenigo, F., et al., *Phosphorylation of VE-cadherin is modulated by haemodynamic forces and contributes to the regulation of vascular permeability in vivo.* Nat Commun, 2012. **3**: p. 1208.

52. Angelini, D.J., et al., *TNF-alpha increases tyrosine phosphorylation of vascular endothelial cadherin and opens the paracellular pathway through fyn activation in human lung endothelia.* Am J Physiol Lung Cell Mol Physiol, 2006. **291**(6): p. L1232-45.

53. Su, W. and A.P. Kowalczyk, *The VE-cadherin cytoplasmic domain undergoes proteolytic processing during endocytosis.* Mol Biol Cell, 2017. **28**(1): p. 76-84.

54. Watanabe, H., et al., *An essential role of myosin light-chain kinase in the regulation of agonist- and fluid flow-stimulated Ca2+ influx in endothelial cells.* FASEB J, 1998. **12**(3): p. 341-8.

55. Tiruppathi, C., et al., *Role of Ca2+ signaling in the regulation of endothelial permeability.* Vascul Pharmacol, 2002. **39**(4-5): p. 173-85.

56. Umapathy, N.S., et al., *Molecular mechanisms involved in adenosine-induced endothelial cell barrier enhancement.* Vascul Pharmacol, 2010. **52**(5-6): p. 199-206.

57. Bhowmick, S., et al., *Impairment of pericyte-endothelium crosstalk leads to blood-brain barrier dysfunction following traumatic brain injury.* Exp Neurol, 2019. **317**: p. 260-270.

58. Chiba, H., et al., *The region-selective regulation of endothelial claudin-5 expression and signaling in brain health and disorders.* J Cell Physiol, 2021.

59. Greene, C. and M. Campbell, *Tight junction modulation of the blood brain barrier: CNS delivery of small molecules.* Tissue Barriers, 2016. **4**(1): p. e1138017.

60. Clark, P.R., et al., *Tumor necrosis factor disrupts claudin-5 endothelial tight junction barriers in two distinct NF-kappaB-dependent phases.* PLoS One, 2015. **10**(3): p. e0120075.

61. Taddei, A., et al., *Endothelial adherens junctions control tight junctions by VE-cadherin-mediated upregulation of claudin-5.* Nat Cell Biol, 2008. **10**(8): p. 923-34.

62. Seok, H., et al., *MicroRNA Target Recognition: Insights from Transcriptome-Wide Non-Canonical Interactions.* Mol Cells, 2016. **39**(5): p. 375-81.

63. Ghafouri-Fard, S., H. Shoorei, and M. Taheri, *Role of microRNAs in the development, prognosis and therapeutic response of patients with prostate cancer.* Gene, 2020. **759**: p. 144995.

64. Hirschberger, S., L.C. Hinske, and S. Kreth, *MiRNAs: dynamic regulators of immune cell functions in inflammation and cancer.* Cancer Lett, 2018. **431**: p. 11-21.

65. Xiao, C. and K. Rajewsky, *MicroRNA control in the immune system: basic principles.* Cell, 2009. **136**(1): p. 26-36.

66. Hayes, J., P.P. Peruzzi, and S. Lawler, *MicroRNAs in cancer: biomarkers, functions and therapy.* Trends Mol Med, 2014. **20**(8): p. 460-9.

67. Adams, B.D., et al., *Targeting noncoding RNAs in disease.* J Clin Invest, 2017. **127**(3): p. 761-771.

68. Lodish, H.F., et al., *Micromanagement of the immune system by microRNAs.* Nat Rev Immunol, 2008. **8**(2): p. 120-30.

69. Ha, M. and V.N. Kim, *Regulation of microRNA biogenesis.* Nat Rev Mol Cell Biol, 2014. **15**(8): p. 509-24.

70. Kreth, S., M. Hubner, and L.C. Hinske, *MicroRNAs as Clinical Biomarkers and Therapeutic Tools in Perioperative Medicine.* Anesth Analg, 2018. **126**(2): p. 670-681.

71. Neudecker, V., et al., *Emerging Roles for MicroRNAs in Perioperative Medicine.* Anesthesiology, 2016. **124**(2): p. 489-506.

72. Muqbil, I., et al., *Nuclear export mediated regulation of microRNAs: potential target for drug intervention.* Curr Drug Targets, 2013. **14**(10): p. 1094-100.

73. Annese, T., et al., *microRNAs Biogenesis, Functions and Role in Tumor Angiogenesis.* Front Oncol, 2020. **10**: p. 581007.

74. Suarez, Y., et al., *Cutting edge: TNF-induced microRNAs regulate TNF-induced expression of E-selectin and intercellular adhesion molecule-1 on human endothelial cells: feedback control of inflammation.* J Immunol, 2010. **184**(1): p. 21-5.

75. Sun, X., N. Belkin, and M.W. Feinberg, *Endothelial microRNAs and atherosclerosis.* Curr Atheroscler Rep, 2013. **15**(12): p. 372.

76. Chamorro-Jorganes, A., E. Araldi, and Y. Suarez, *MicroRNAs as pharmacological targets in endothelial cell function and dysfunction.* Pharmacol Res, 2013. **75**: p. 15-27.

77. Marin, T., et al., *Mechanosensitive microRNAs-role in endothelial responses to shear stress and redox state.* Free Radic Biol Med, 2013. **64**: p. 61-8.

78. Young, J.A., et al., *Regulation of vascular leak and recovery from ischemic injury by general and VE-cadherin-restricted miRNA antagonists of miR-27.* Blood, 2013. **122**(16): p. 2911-9.

79. Gu, W., et al., *MicroRNA-22 regulates inflammation and angiogenesis via targeting VE-cadherin.* FEBS Lett, 2017. **591**(3): p. 513-526.

80. Mishra, R. and S.K. Singh, *HIV-1 Tat C modulates expression of miRNA-101 to suppress VE-cadherin in human brain microvascular endothelial cells.* J Neurosci, 2013. **33**(14): p. 5992-6000.

81. Guo, J., et al., *Role of linc00174/miR-138-5p (miR-150-5p)/FOSL2 Feedback Loop on Regulating the Blood-Tumor Barrier Permeability.* Mol Ther Nucleic Acids, 2019. **18**: p. 1072-1090.

82. Rajput, C., et al., *MicroRNA-150 Suppression of Angiopoetin-2 Generation and Signaling Is Crucial for Resolving Vascular Injury.* Arterioscler Thromb Vasc Biol, 2016. **36**(2): p. 380-8.

83. Zhuang, Y., et al., *MicroRNA Regulation of Endothelial Junction Proteins and Clinical Consequence.* Mediators Inflamm, 2016. **2016**: p. 5078627.

84. Potenza, N. and A. Russo, *Biogenesis, evolution and functional targets of microRNA-125a.* Mol Genet Genomics, 2013. **288**(9): p. 381-9.

85. Li, D., et al., *MicroRNA-125a/b-5p inhibits endothelin-1 expression in vascular endothelial cells.* J Hypertens, 2010. **28**(8): p. 1646-54.

86. Muramatsu, F., et al., *microRNA-125b inhibits tube formation of blood vessels through translational suppression of VE-cadherin.* Oncogene, 2013. **32**(4): p. 414-21.

87. Zhao, D., et al., *Plasma miR-125a and miR-125b in sepsis: Correlation with disease risk, inflammation, severity, and prognosis.* J Clin Lab Anal, 2020. **34**(2): p. e23036.

88. Mitchell, P.S., et al., *Circulating microRNAs as stable blood-based markers for cancer detection.* Proc Natl Acad Sci U S A, 2008. **105**(30): p. 10513-8.

89. Garo, L.P. and G. Murugaiyan, *Contribution of MicroRNAs to autoimmune diseases.* Cell Mol Life Sci, 2016. **73**(10): p. 2041-51.

90. Valadi, H., et al., *Exosome-mediated transfer of mRNAs and microRNAs is a novel mechanism of genetic exchange between cells.* Nat Cell Biol, 2007. **9**(6): p. 654-9.

91. Piccin, A., W.G. Murphy, and O.P. Smith, *Circulating microparticles: pathophysiology and clinical implications.* Blood Rev, 2007. **21**(3): p. 157-71.

92. Joop, K., et al., *Microparticles from patients with multiple organ dysfunction syndrome and sepsis support coagulation through multiple mechanisms.* Thromb Haemost, 2001. **85**(5): p. 810-20.

93. Delabranche, X., et al., *Microparticles are new biomarkers of septic shock-induced disseminated intravascular coagulopathy.* Intensive Care Med, 2013. **39**(10): p. 1695-703.

94. Ge, Y., et al., *MicroRNA-125a suppresses intestinal mucosal inflammation through targeting ETS-1 in patients with inflammatory bowel diseases.* J Autoimmun, 2019. **101**: p. 109-120.

95. Guo, S., et al., *Complex oncogene dependence in microRNA-125a-induced myeloproliferative neoplasms.* Proc Natl Acad Sci U S A, 2012. **109**(41): p. 16636-41.

96. Vallet, B., *Bench-to-bedside review: endothelial cell dysfunction in severe sepsis: a role in organ dysfunction?* Crit Care, 2003. **7**(2): p. 130-8.

97. Schlegel, N. and J. Waschke, *cAMP with other signaling cues converges on Rac1 to stabilize the endothelial barrier- a signaling pathway compromised in inflammation.* Cell Tissue Res, 2014. **355**(3): p. 587-96.

98. Fosse, J.H., et al., *Endothelial Cells in Emerging Viral Infections.* Front Cardiovasc Med, 2021. **8**: p. 619690.

99. Chousterman, B.G., F.K. Swirski, and G.F. Weber, *Cytokine storm and sepsis disease pathogenesis.* Semin Immunopathol, 2017. **39**(5): p. 517-528.

100. Caolo, V., et al., *Shear Stress and VE-Cadherin.* Arterioscler Thromb Vasc Biol, 2018. **38**(9): p. 2174-2183.

101. Vion, A.C., et al., *Endothelial Cell Orientation and Polarity Are Controlled by Shear Stress and VEGF Through Distinct Signaling Pathways.* Front Physiol, 2020. **11**: p. 623769.

102. Hermann, S., et al., *Diagnostic potential of circulating cell-free microRNAs for community-acquired pneumonia and pneumonia-related sepsis.* J Cell Mol Med, 2020. **24**(20): p. 12054-12064.

103. Reithmair, M., et al., *Cellular and extracellular miRNAs are blood-compartment-specific diagnostic targets in sepsis.* J Cell Mol Med, 2017. **21**(10): p. 2403-2411.

104. Lee, H., et al., *Caveolin-1 selectively regulates microRNA sorting into microvesicles after noxious stimuli.* J Exp Med, 2019. **216**(9): p. 2202-2220.

105. Uray, K., E. Major, and B. Lontay, *MicroRNA Regulatory Pathways in the Control of the Actin-Myosin Cytoskeleton.* Cells, 2020. **9**(7).

106. Ichimura, A., et al., *miRNAs and regulation of cell signaling.* FEBS J, 2011. **278**(10): p. 1610-8.

107. Vittet, D., et al., *Targeted null-mutation in the vascular endothelial-cadherin gene impairs the organization of vascular-like structures in embryoid bodies.* Proc Natl Acad Sci U S A, 1997. **94**(12): p. 6273-8.

108. Montero-Balaguer, M., et al., *Stable vascular connections and remodeling require full expression of VE-cadherin in zebrafish embryos.* PLoS One, 2009. **4**(6): p. e5772.

109. Nachtigal, P., A. Gojova, and V. Semecky, *The role of epithelial and vascular-endothelial cadherin in the differentiation and maintenance of tissue integrity*. Acta Medica (Hradec Kralove), 2001. **44**(3): p. 83-7.

110. Wheelock, M.J. and K.R. Johnson, *Cadherin-mediated cellular signaling.* Curr Opin Cell Biol, 2003. **15**(5): p. 509-14.

111. Liebner, S., U. Cavallaro, and E. Dejana, *The multiple languages of endothelial cell-to-cell communication.* Arterioscler Thromb Vasc Biol, 2006. **26**(7): p. 1431-8.

112. Gareri, C., et al., *miR-125a-5p Modulates Phenotypic Switch of Vascular Smooth Muscle Cells by Targeting ETS-1.* J Mol Biol, 2017. **429**(12): p. 1817-1828.

113. Nakamura, Y., et al., *Role of protein tyrosine phosphatase 1B in vascular endothelial growth factor signaling and cell-cell adhesions in endothelial cells.* Circ Res, 2008. **102**(10): p. 1182-91.

114. Walsh, J.E. and M.R. Young, *Interrelationship between protein phosphatase 1 and TGF-{beta} in regulating motility and cytoskeletal architecture of endothelial cells.* Anticancer Res, 2010. **30**(12): p. 4861-6.

115. Boratko, A. and C. Csortos, *PKC mediated phosphorylation of TIMAP regulates PP1c activity and endothelial barrier function.* Biochim Biophys Acta Mol Cell Res, 2017. **1864**(2): p. 431-439.

116. Kim, K.M., et al., *Molecular characterization of myosin phosphatase in endothelium.* J Cell Physiol, 2012. **227**(4): p. 1701-8.

117. Peter, M.E., *Targeting of mRNAs by multiple miRNAs: the next step.* Oncogene, 2010. **29**(15): p. 2161-4.

118. Ludwig, N., et al., *Distribution of miRNA expression across human tissues.* Nucleic Acids Res, 2016. **44**(8): p. 3865-77.

119. Contreras, J. and D.S. Rao, *MicroRNAs in inflammation and immune responses.* Leukemia, 2012. **26**(3): p. 404-13.

120. Lee, L.K., et al., *The Role of MicroRNAs in Acute Respiratory Distress Syndrome and Sepsis, From Targets to Therapies: A Narrative Review.* Anesth Analg, 2020. **131**(5): p. 1471-1484.

121. Lima, J.F., et al., *Anti-miRNA oligonucleotides: A comprehensive guide for design.* RNA Biol, 2018. **15**(3): p. 338-352.

122. Connelly, C.M. and A. Deiters, *Identification of inhibitors of microRNA function from small molecule screens.* Methods Mol Biol, 2014. **1095**: p. 147-56.

123. Zhang, J., et al., *miRspongeR: an R/Bioconductor package for the identification and analysis of miRNA sponge interaction networks and modules.* BMC Bioinformatics, 2019. **20**(1): p. 235.

124. Lu, L.H., C.H. Chao, and T.M. Yeh, *Inhibition of autophagy protects against sepsis by concurrently attenuating the cytokine storm and vascular leakage.* J Infect, 2019. **78**(3): p. 178-186.

125. Ma, S., et al., *Endothelial bioreactor system ameliorates multiple organ dysfunction in septic rats.* Intensive Care Med Exp, 2016. **4**(1): p. 23.

126. Goldenberg, N.M., et al., *Broken barriers: a new take on sepsis pathogenesis.* Sci Transl Med, 2011. **3**(88): p. 88ps25.

Acknowledgement

The completion of this dissertation is inseparable from the selfless help of many people. I would like to take the opportunity to thank you all for supporting me during my three years of Ph.D.

First and foremost, I want to thank Prof. Simone Kreth, who has been a great supervisor, for inspiring, guiding, advising when I encountered difficulties. Thank you for giving me the precious opportunity to study at LMU and opening the door to a new life in scientific research for me. This dissertation has benefited a lot from your precise comments and suggestions. I would like to take this opportunity to thank my mentor and guide, Dr. Martin Müller. He patiently provided encouragement and advice throughout my Ph.D. I enjoyed working with you, as you are not only an excellent researcher but also an equally great teacher. Your enthusiasm for scientific research has deeply infected me.

I want to thank the entire research team for the cooperative atmosphere and helpfulness. Especially, I would like to thank Dr. Max Hübner, Dr. David Effinger and Tingting Wu for your help, advice, and scientific discussions. My sincere thanks to my co-worker Valena Ließke for your fast and reliable work for this study and taught me lab methods. To Gaby and Gudrun, many thanks for your help and support to me, both in the experiment and in life. You made the foreign life much easier for me while simultaneously ensuring a warm-hearted working atmosphere at the Walter Brendel Centre of Experimental Medicine.

The great support during this time came from friends back home and friends I got to know in Germany. Thank you very much for your encouragement during those difficult periods of my Ph.D. study.

I would like to express my heartfelt gratitude to my parents for their never-ending support and encouragement throughout my life. Thanks to my husband, Chao. Thank

you for your enormous dedication, making me happy and laughing, and thank you for your love and affection.

Finally, I do not want to miss this opportunity to thank all members of my doctoral committee who gave time and interest to my project. Thanks to China Scholarship Council for providing me the PhD-scholarship during my study.

Affidavit

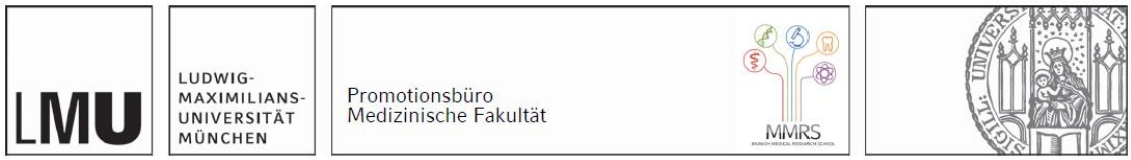

Affidavit

Li, Lei
Surname, first name

Street

Zip code, town, country

I hereby declare, that the submitted thesis entitled:

A Micro-RNA-125a-Driven Functional Network Promotes Endothelial Permeability in Acute Inflammatory Conditions

is my own work. I have only used the sources indicated and have not made unauthorized use of services of a third party. Where the work of others has been quoted or reproduced, the source is always given.
I further declare that the submitted thesis or parts thereof have not been presented as part of an examination degree to any other university.

Hohhot, China 14.08.2022
Place, date

Lei Li
Signature doctoral candidate

Confirmation of congruency

Confirmation of congruency between printed and electronic version of the doctoral thesis

Li, Lei

Surname, first name

Street

Zip code, town, country

I hereby declare, that the submitted thesis entitled:

A Micro-RNA-125a-Driven Functional Network Promotes Endothelial Permeability in Acute Inflammatory Conditions

is congruent with the printed version both in content and format.

Hohhot, China 14.08.2022

Place, date

Lei Li

Signature doctoral candidate